Analysis of within and between-GCM uncertainties of runoff projections in Mediterranean-like catchments

Pilar A. Barria[1,2], Murray C. Peel[3], Kevin J.E. Walsh[1], René Garreaud[4]

(Manuscript received October 2017; accepted December 2017)

[1] School of Earth Sciences, University of Melbourne, Melbourne, Australia

[2] International Hydrology Research Group, Faculty of Forest Sciences and Nature Conservancy, University of Chile, Santiago, Chile

[3] Department of Infrastructure Engineering, University of Melbourne, Melbourne, Australia

[4] Geophysics Department, Facultad de Ciencias Físicas y Matemáticas, Universidad de Chile, Santiago, Chile

Corresponding author's address: Pilar Barria, School of Earth Sciences, University of Melbourne 3010 Victoria, Australia. E-mail: pbarria@student.unimelb.edu.au

Abstract

Streamflow reductions have been reported in mid-latitude Southern Hemisphere (SH) catchments, in particular in the southwest of Western Australia (SWA) and in central Chile (CC), following decreases in precipitation since the mid-1970s. Although projections from Global Climate Models (GCMs) indicate the observed trends are expected to continue during the rest of the 21st century, they are affected by large uncertainties that challenge informed decision making. Quantification and comparison of uncertainties in runoff projections for the period 2050-2080 relative to 1970-2000, driven by an ensemble of a single GCM with perturbed physics (CPDN) and a multi-model ensemble of different GCMs (CMIP5), were used to account for what we term "within-GCM" and "between-GCM" uncertainty in SWA catchments. Between-GCM uncertainty of runoff projections was also quantified in CC catchments. Within and between-GCM uncertainties were found to be very similar (~55 per cent) in SWA catchments. Between-GCM uncertainty for runoff projections in CC catchments is smaller than in SWA. On average, uncertainty of about 51 per cent, under RCP8.5 scenario, was simulated for the period 2050-2080 compared to 1970-2000. For CC catchments a dichotomy was observed in runoff projections under the RCP4.5 scenario, which according to our preliminary analysis might relate to how ozone is specified within different GCMs. We conclude that the number of models sampled by the CMIP5 ensemble, which includes multiple model runs from some GCMs, provides some insight into within-GCM uncertainties. Furthermore, since CMIP5 model runs report values for all regions and are easily accessible, the CMIP5 ensemble is more convenient for regional hydrological assessments than the perturbed physics experiments.

1. Introduction

We are living in a warmer world, with the IPCC 5th Assessment Report (Stocker et al., 2013) stating that global mean surface temperature increased by about 0.89°C over the period 1901 to 2012. Although changes in temperature affect the global hydrological cycle, regional changes in surface hydroclimatology are very variable and uncertain compared to those in temperature (Milly et al., 2005, Stocker et al., 2013). Nevertheless, in Southern Hemisphere extratropical regions, like southwest Western Australia (SWA) and central Chile (CC), sustained increases in temperature and reductions in precipitation have led to reductions in streamflow (Magrin et al., 2014, Reisinger et al., 2014). These changes in temperature and precipitation are projected to continue to reduce streamflow into the future (Prosser, 2011, Teng et al., 2012, Demaria et al., 2013, Samaniego et al., 2009, Prudhomme et al., 2014, Bozkurt et al., 2017, Vicuña et al., 2013), which would endanger water availability in these regions.

Future water resources availability is commonly assessed by running a hydrological model driven by projections from global climate models (GCMs). Uncertainties in these projections arise from three main sources: the GCM used for simulating the future climatic variables (temperature and precipitation), the downscaling methodology used to translate the variables to the catchment scale and the hydrological model used to estimate runoff. The GCM projections of the climatic variables represent the foremost source of uncertainty (Ardoin-Bardin et al., 2009, Chiew et al., 2008, Chiew et al., 2009, Prudhomme and Davies, 2009a, Prudhomme and Davies, 2009b, Xu et al., 2011, Bosshard et al., 2013, Sonnenborg et al., 2015).

According to, Hawkins and Sutton (2011), Hawkins and Sutton (2009) and Woldemeskel et al. (2016), the GCM uncertainties can in turn be partitioned into three groups. First, uncertainties result from the wide range of possible future anthropogenic forcing paths, which have been addressed by the definition of different emission scenarios (Moss et al., 2010). Second, uncertainties arise from the model representation of the climatic system, enhanced by an inadequate understanding of some atmospheric processes such as aerosol-cloud interactions and changes in the components of the water cycle (Stocker et al., 2013). Finally, the random internal variability of the climate system, i.e. the natural fluctuations of the climate system, are an inherent source of climatological uncertainty in both models and observations.

Two main approaches have been used to quantify the effects of GCM uncertainties on runoff projection studies which we term “between-GCMs” and “within-GCMs” uncertainties (Parker, 2013, Peel et al., 2015). The between-GCMs analysis of uncertainty considers the spread of a multi-model ensemble of different GCM projections for a given emissions scenario as a first order uncertainty; it quantifies the uncertainty due to different GCM formulations. The IPCC assessments and the GCM runs collated by the Coupled Model Intercomparison Project Phase 3 (CMIP3; Meehl et al. (2007)) and Phase 5 (CMIP5; Taylor et al. (2012)) are the main sources of data that researchers have used in multi-model or between-GCMs analyses. Nevertheless, Mote et al. (2011) emphasizes that the range of different model runs in CMIP3 and CMIP5 are not intended to represent the physical uncertainty in climatic projections, but to examine the consensus in them. A notable amount of research about uncertainties of runoff projections has relied upon these ensembles of GCM runs (Bosshard et al., 2013, Dobler et al., 2012, Lafaysse et al., 2014, Steinschneider et al., 2012).

Within-GCM uncertainty is defined here as the range of possible projections from a single model for a given emissions scenario for either a single set of parameter values that represent the physics within the GCM or from a plausible range of the GCM parameter values. Within-GCM uncertainty includes both internal variability and initial condition uncertainty. To date, the only large ensemble of long-term projection data to investigate within-GCM uncertainty is the climateprediction.net (CPDN) project (Rowlands et al., 2012), which through variations of the parameters that represent the physics of the model has quantified the GCM uncertainty (Mote et al., 2011, Stainforth et al., 2005). Barria et al. (2015) performed the first hydrologic assessment of the impacts of within-GCM uncertainty on runoff projections using the perturbed physics runs from CPDN for three catchments in SWA and found that projected runoff reductions by 2050-2080 under the A1B scenario (Nakicenovic et al., 2000) range between 10 per cent and 80 per cent compared to the historical period (1970-2000).

The present study seeks to extend the Barria et al. (2015) assessment, addressing both the between-GCM and within-GCM uncertainties of runoff projections for Mediterranean-like catchments located in SWA and CC, where similar climatic trends have been observed. Runoff projections were obtained by running a

lumped hydrological model, the Precipitation Evaporation Runoff model (PERM; Peel et al. (2015)) forced by bias corrected CMIP5 and CPDN runs. This comparison aims to provide quantitative information about the impact of within-GCM and between-GCM uncertainties on projected runoff to inform water management adaptation measures. Second, the comparison seeks to identify whether the number of multiple model runs in the CMIP5 ensemble adequately represents within-GCM uncertainty. If it does, then future hydrologic assessments of within-GCM uncertainty in extratropical regions could use CMIP5 model runs, which cover the world and are easily accessible, rather than CPDN. Further information about these ensembles of GCM runs is presented in the Data section. Since the CPDN data were saved and released over Giorgi regions (Giorgi et al., 2001), which are too coarse for representing the steep topography and resulting complex CC climate, only CMIP5 GCM runs were used in this area. Thereby, we aim to extend the analysis performed in SWA to CC, quantifying how much runoff is expected to change by the second half of the century in the region, including the analysis of the uncertainties around those projections.

1.1 Study regions

Uncertainties in runoff projections in six catchments in SWA and CC have been studied. From north to south, Helena river at Ngangaguringuring, Donnelly river at Strickland and Denmark river at Kompup were modeled in SWA; and from north to south, Cauquenes river at El Arrayan, Cato river at Puente Cato and Lumaco river at Lumaco have been assessed in CC. The main characteristics of the six catchments are presented in Table 1 and a map with their location is presented in Figure 1a and 1b for SWA and CC respectively.

Table 1 Characteristics of the SWA and CC catchments

Catchment	*Region*	*Period of observations*	*Area (km^2)*	*Mean annual precipitation (mm/year)*	*Mean annual temperature (ºC)*	*Mean annual runoff (mm/year)*	*Standard deviation of annual runoff (mm/year)*	*CV*
Donnelly at Strickland	SWA	1961-1992	780	1004	15.2	162.72	69.8	0.43
Helena at Ngangaguringuring	SWA	1973-2000	327	665	17	6.41	5.6	0.87
Denmark at Kompup	SWA	1961-2000	502	835	15.3	58.93	34.3	0.58
Cauquenes en el Arrayán	CC	1966-2000	619	715	8.7	463.6	260.4	0.56
Cato en Puente Cato	CC	1966-2005	987	1694	8.7	1297.2	489.7	0.38
Lumaco en Lumaco	CC	1966-2005	869	1053	10.1	620.6	198.4	0.32

SWA has a temperate, Mediterranean climate with a dry and hot summer and wet winter (Peel et al., 2007). SWA catchments are rainfall dominated: the maximum runoff and maximum rainfall are observed during austral winter months (June-August). Precipitation in this region is driven by mid-latitude frontal systems associated with the position of the subtropical ridge and ranges from around 1200 mm per year in the coastal areas to around 500 mm per year in the north (Silberstein et al., 2012). The Southern Annular Mode (SAM), a mode of the north-south variability of the westerly wind belt, has been associated with the interannual variability of precipitation in this region, while the El Niño Southern Oscillation (ENSO) has a secondary impact (Hendon et al., 2007, Nicholls, 2009, Hope et al., 2015).

Reduced winter precipitation of around 10-15 per cent has been detected since the mid-1970's in SWA by several researchers (Charles et al., 2010, Frederiksen and Frederiksen, 2007, Hennessy et al., 2007, IOCI, 2012, Timbal, 2004). This reduced precipitation has led to reductions of average inflows to reservoirs of

about half historical levels (1911-1973). One likely cause of the reduction in precipitation is the increasing trend in mean sea level pressure over SWA linked to a positive trend in the SAM (Allan and Haylock, 1993, Cai and Cowan, 2006, Delworth and Zeng, 2014, IOCI, 2012). Runoff reductions are projected to continue during the 21st century in SWA (Hope et al., 2015, Silberstein et al., 2012, Preston and Jones, 2008, Barria et al., 2015). However, uncertainties around these projections have not been comprehensively quantified.

Figure 1 Map presenting a) Location of the Southwest Western Australian catchments and b) Central Chilean catchments.

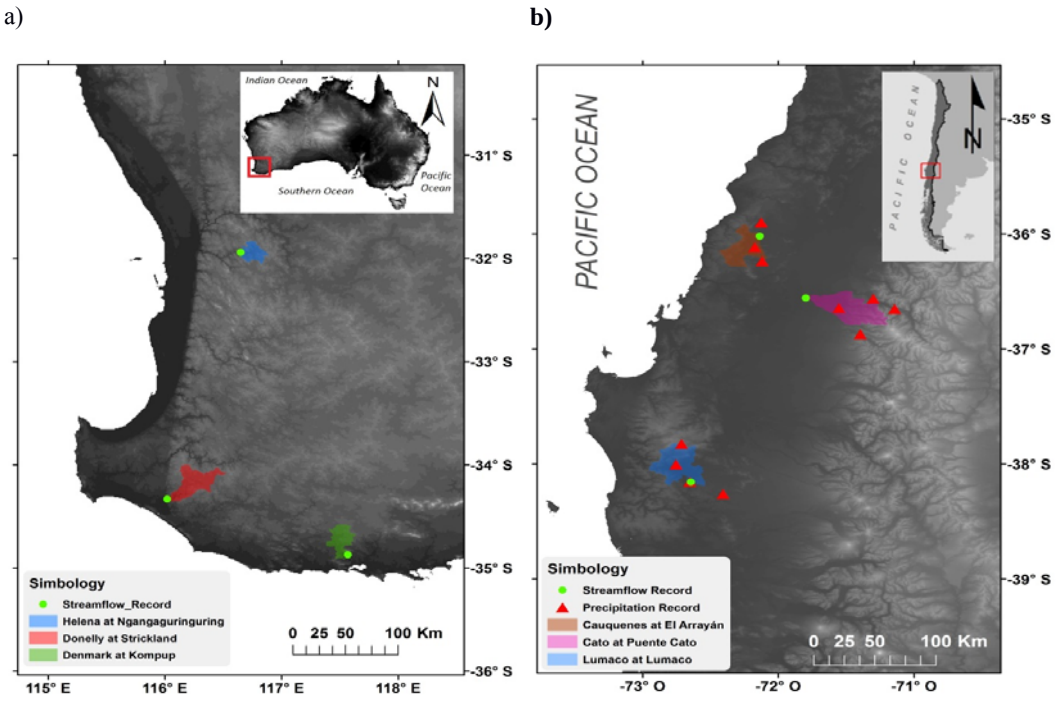

CC is the land area located between latitudes 35ºS and 39ºS on the west slopes of the Andes (Figure 1b). Like SWA, CC has a temperate climate with a dry and warm summer and wet and cold winter (Peel et al., 2007). Similar to the SWA catchments, the three study catchments in CC have a pluvial regime of runoff with a maximum during winter months when precipitation is maximum (Cortés et al., 2011). No snowmelt dominated runoff catchments were analysed in this study. Precipitation in CC is mainly generated by warm and cold fronts associated with migratory surface cyclones (Falvey and Garreaud, 2007) and ranges between around 500 to 2500 mm yr^{-1} (Rubio and McPhee, 2010). Precipitation at the Cordillera mountain range is around two to three times the amount observed in coastal areas due to orographic enhancement (Falvey and Garreaud, 2009, Viale and Garreaud, 2015).

According to Quintana and Aceituno (2012) and Rubio and McPhee (2010), two different patterns of precipitation and runoff have been observed in the region with a boundary at around 37°S. ENSO and its multidecadal variability modulated by the Pacific Decadal Oscillation (PDO; Trenberth and Hurrell (1994)) dominates the interannual variability in the region north of 37°S, while the SAM has a major influence on the interannual variability of the region located south of 37°S (Garreaud, 2009).

Since the mid-1970s, reductions in CC precipitation (Carrasco et al., 2008, Boisier et al., 2016) and runoff (MOP, 2012, Rubio and McPhee, 2010) have been detected which have been associated with a shift in the PDO cycle identified in 1976/1977 (Fuenzalida et al., 2007). A prolonged deficit in precipitation (30 per cent below the 1970-2000 climatology) has been observed in central Chile since 2010, which has been called the "megadrought" (Boisier et al., 2016). Current water scarcity conditions along with projections of runoff reductions during the following decades (Demaria et al., 2013, Fuenzalida et al., 2007, Bozkurt et al., 2017) enhance the need for a more comprehensive analysis of the uncertainty of runoff projections in CC catchments.

2. Data

2.1 GCM data

Monthly temperature and precipitation data from the GCMs collated by the CPDN and CMIP5 ensembles were used in this assessment. CPDN uses the HadCM3L model, a reduced ocean resolution version of the HadCM3 model (Gordon et al., 2000), which through perturbed physics was run 2500 times generating climatic simulations for the period between 1920 until 2080 (Rowlands et al., 2012). The resolution of the model is 2.5º latitude by 3.75º longitude with 19 vertical levels in the atmosphere and 2.5º latitude by 3.75º longitude and 20 vertical levels in the ocean (Rowland et al., 2012). Each individual ensemble member was run under control forcing (pre-industrial or representative of 1900 conditions) and transient forcing (time-varying concentrations of greenhouse gases) for the period between 1920 and 2080. CPDN was run under the A1B scenario (Nakicenovic et al., 2000), which specifies the emissions of greenhouse gases and aerosols for an assumed future world of rapid economic growth.

A list of the 106 simulations from the 41 CMIP5 GCMs used in this analysis, along with the GCMs characteristics, are presented in Table S1. The CMIP5 ensemble mainly provides insight into between-GCM uncertainty. However, as some GCMs have multiple runs, the ensemble also provides some insight into within-GCM uncertainty. CMIP5 models were run under control forcings (pre-industrial or representative of 1900 conditions) for the period between 1900 and 2005 and transient forcing (time-varying concentrations of greenhouse gases) for the period between 2006 and 2100. The anthropogenic forcing scenarios considered in this study correspond to the RCP4.5 (Van Vuuren et al., 2011), which is a moderate scenario that assumes a path of emissions that peaks by 2040 and then starts decreasing. We also evaluated the RCP8.5 scenario (Van Vuuren et al., 2011) which assumes that emissions continuing to rise thorough to 2100, which gives a more risk-averse perspective regarding future runoff reductions. The CMIP5 data were resampled to a resolution of 1.5° latitude by 1.5° longitude and were provided by the Australian Bureau of Meteorology (F. Delage, personal communication, October, 9, 2015).

2.2 Observed climatological data

Gridded monthly observed precipitation and temperature data for the SWA catchments were obtained from the Australian Water Availability Project (AWAP; Jones et al. (2009)). AWAP uses in-situ observations and provides gridded data at a spatial resolution of 0.05º x 0.05º, which we averaged to a 0.25 º x 0.25º grid for our analysis.

Monthly rain gauge and temperature data for the CC catchments were obtained from the records of two Chilean agencies: the Directorate of Water Resources (Dirección General de Aguas, DGA) and the Weather Service (Dirección Meteorológica de Chile, DMC). Information about the meteorological stations used in this study is presented in Table S2 in the Supplementary Material, four stations were used to characterise the Cauquenes catchment, three for the Cato catchments and four for Lumaco catchment (Fig. 1b).

ARCGIS 9.3 was used to delineate the catchment boundaries using the two-second Shuttle Radar Topography Mission (SRTM) Smoothed Digital Elevation Model (DEM-S) version 1.0 (Geoscience Australia, 2010) for Australia and the ASTER Global DEM (ASTER, 2009) for CC catchments. Area-weighted temperature and precipitation values were calculated for each catchment.

2.3 Runoff data

The monthly runoff data used to calibrate the hydrological model for the SWA catchments were taken from the stream gauging sites monitored by the Western Australian government's Department of Water (see the Government of Western Australia, Department of Water, at http://wir.water.wa.gov.au/SitePages/SiteExplorer.aspx). The Chilean monthly runoff data were obtained from the Directorate of Water Resources (Dirección General de Aguas, DGA).

The characteristics of the six runoff stations studied here are presented in Table 1. The seasonal pattern of runoff for the six catchments is presented in the Supplementary Material Figure S3, which confirms that all catchments present a pluvial runoff regime with an absence of a snow melting season.

3. Methodology

Runoff projections and uncertainty quantification for the second half of the century in the three SWA and three CC catchments were assessed through a three stage methodology, presented in Figure 2 and described below.

Figure 2 Methodology scheme

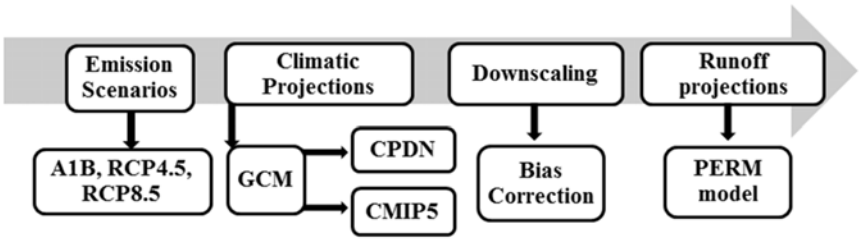

3.1 Bias correction methodology

A statistical downscaling methodology was used to translate the spatially coarse outputs from the GCMs (hundreds of km^2) to the catchment scale. We apply a direct and parameter free Quantile-Quantile methodology (Themeßl et al., 2011), which matches the empirical cumulative distribution function (*ecdf*) of the GCM data to the *ecdf* of the observed data in every catchment on a monthly basis following the equations presented below:

$$Y_{t,cat}^{cor} = X_{t,cat}^{raw} + CF_{t,cat}$$

$$CF_{t,cat} = ecdf_{moy,cat}^{obs,cal-1}\left(P_{t,cat}\right) - ecdf_{moy,cat}^{mod,cal-1}\left(P_{t,cat}\right)$$

$$P_{t,cat} = ecdf_{moy,cat}^{mod,cal}\left(X_{t,cat}^{raw}\right)$$

where $Y_{t,cat}^{cor}$ refers to the bias corrected (*cor*) precipitation or temperature GCM output over a catchment (*cat*) in a particular month *t*. $X_{t,cat}^{raw}$ is the raw precipitation or temperature GCM output over a catchment for the same month *t*. The $ecdf_{moy,cat}^{obs,cal-1}$ is the inverse empirical cumulative distribution function of the observed (*obs*) and $ecdf_{moy,cat}^{mod,cal-1}$ of the modelled (*mod*) variable under study for a particular month of the year (*moy*) and for every catchment during the calibration period (*cal*). The difference between the inverse *ecdf* of the observed and the modelled variable for every month and every catchment is the correction factor, or the bias correction that is then applied to the simulations.

3.2 PERM model

A lumped conceptual hydrological model was used to simulate monthly runoff using the monthly bias corrected precipitation and temperature data from the GCMs. The precipitation, evaporation, runoff model (PERM) was developed and described by Peel et al. (2015). A diagram of the model stores and fluxes is presented in Figure 3.

Figure 3 PERM model diagram (from Peel et al., 2015)

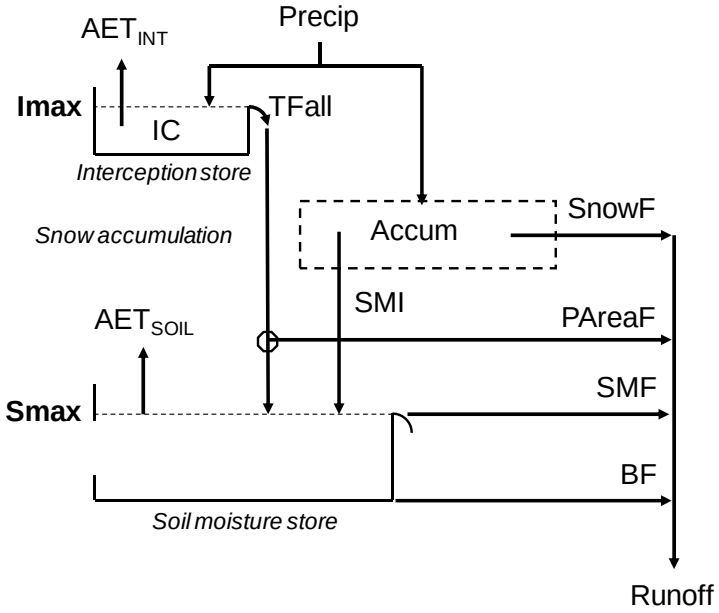

The model comprises three storages: the Interception store (IC), the soil moisture store (SMS) and the snow accumulation storage (ACCUM). Five parameters are calibrated using observed monthly precipitation, temperature and runoff data, which influence model fluxes and stores: the rate of snowmelt and potential evapotranspiration (ETrate, mm/°C/month), the proportion of snowmelt volume to runoff (Melt), the soil moisture storage capacity (Smax, mm), the baseflow linear recession parameter (K) and the interception storage capacity (Imax, mm). PERM calculates runoff as the addition of snowmelt flow, saturated partial area flow (PAreaF), soil moisture excess flow (SMF) and baseflow (BF) through a volume balance. More details are provided in Peel et al. (2015).

The model is calibrated by minimising the sum of squared differences between the estimated and the observed annual runoff. The model performance was assessed using the Nash & Sutcliffe Efficiency value (Nash and Sutcliffe, 1970). A K-Fold cross validation (Efron and Tibshirani, 1993) with K=3 was also used to evaluate the calibrated PERM model for every catchment.

3.3 Within and Between-GCM uncertainties quantifications and comparison

The within and between-GCM uncertainties of projected variables were calculated using the range between the 5th and the 95th percentiles of the change in precipitation or runoff for the period 2050 to 2080 compared to 1970 to 2000. The projected rainfall and temperature were obtained from CPDN and the CMIP5 ensemble of GCM runs.

The two-sided Kolmogorov Smirnov test was used to compare the histograms of change in annual rainfall and runoff using CPDN and CMIP5, to test the hypothesis of whether they are from the same continuous distribution or not.

4. Results

Results of the quantification of GCM-uncertainty of projected runoff for SWA and CC are presented in the following five sub-sections. First, the ability of the raw CPDN and CMIP5 data to simulate the climate of the studied regions during the observed period is evaluated. Then, the calibration and evaluation results of modelled runoff for the six study catchments are shown in the second section. The third section presents the comparison of the effect of the within and between-GCM uncertainties of SWA runoff projections. Only between-GCM uncertainty of runoff projections are analysed for CC, presented in the fourth section.

Finally, a sensitivity of runoff projections in CC to ozone characterisation within the GCM models is presented in section 4.5.

4.1 CMIP5 and CPDN evaluation in SWA and CC catchments

Seasonal precipitation and temperature modelled by the GCM runs in the CMIP5 were compared to observed climatological data in order to evaluate the ability of the GCMs to simulate the climate of SWA and CC. Boxplots of mean and standard deviation of annual precipitation simulated by the CMIP5 GCM ensemble during the observed period along with the mean and standard deviation of observed annual precipitation are presented in Figures 4a and 4b respectively. The evaluation of the mean and standard deviation of annual temperature simulated by CMIP5 GCMs is presented in the Supplementary Material in Figures S4 and S5 respectively.

Figure 4a) Comparison of mean annual precipitation simulated by CMIP5 in the historical period and observed mean annual precipitation. b) Comparison of standard deviation of annual precipitation simulated by CMIP5 in the historical period and standard deviation of observed annual precipitation.

a)

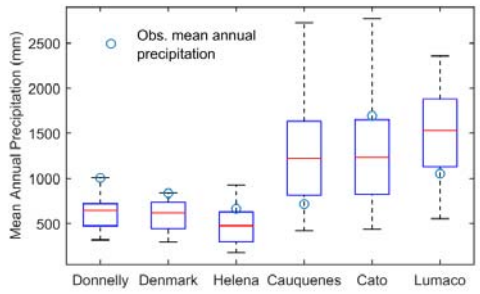

b)

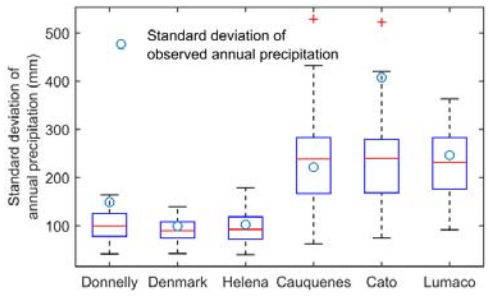

Overall, the CMIP5 GCMs underestimate mean annual precipitation by 31 per cent on average in the SWA catchments. The GCM ensemble is better at representing the variability (annual standard deviation) than the mean of annual precipitation in the SWA catchments, with a 14 per cent underestimation on average. Regarding mean annual temperature, the GCMs tend to overestimate mean annual temperature in SWA catchments. However, the ensemble reproduces the decrease in precipitation and the increase in temperature (not shown) during the observed period (1970-2000). Barria et al. (2015) evaluated the CPDN dataset and found that the perturbed physics ensemble was better at simulating observed temperature (a 1.4 per cent difference in the average of the simulation of the median) than observed precipitation (a 6.2 per cent of difference in the average of the simulation of the median) in the SWA catchments.

The CMIP5 ensemble tends to overestimate mean annual precipitation at the Cauquenes and Lumaco catchments during the observed period (an overestimation of 58 per cent on average) and to underestimate mean annual precipitation for the Cato River (24 per cent). Results presented in Figure 4b indicate that CMIP5 is more accurate at simulating the standard deviation of annual precipitation for the Cauquenes and Lumaco catchments (a 4.7 per cent difference on average), than for the Cato catchment (44 per cent difference). The CMIP5 ensemble is more accurate in simulating the standard deviation than the mean of annual temperature in the CC catchments. Despite the differences between CMIP5 and the observed mean and standard deviation of the annual climatic variables, the ensemble of models did reproduce reductions in precipitation and increases in temperature during the historical period (1970-2000). Larger spatial variability is observed in CC than in SWA which might be related to the larger bias in the GCMs when attempting to simulate steep topography such as in CC.

The monthly GCM precipitation and temperature data for the six catchments were translated to the catchment scale using the quantile-quantile bias correction methodology based in the period in which runoff observations were available in every case (Themeßl et al., 2012), prior to being input to the hydrological model. One example of bias corrected data is presented in Figure 5a and b, where annual precipitation at

Donnelly and Cauquenes catchment respectively is shown. According to Figure 5 the mean and the percentiles of the simulations represented by the blue lines fit the observed annual rainfall over the catchment after using the bias correction methodology. Similar results were found in the other catchments for precipitation and temperature (not shown).

Figure 5 Bias corrected CMIP5 simulated annual precipitation under the RCP8.5 scenario over a) Donnelly at Strickland and b) Cauquenes at El Arrayán

a)

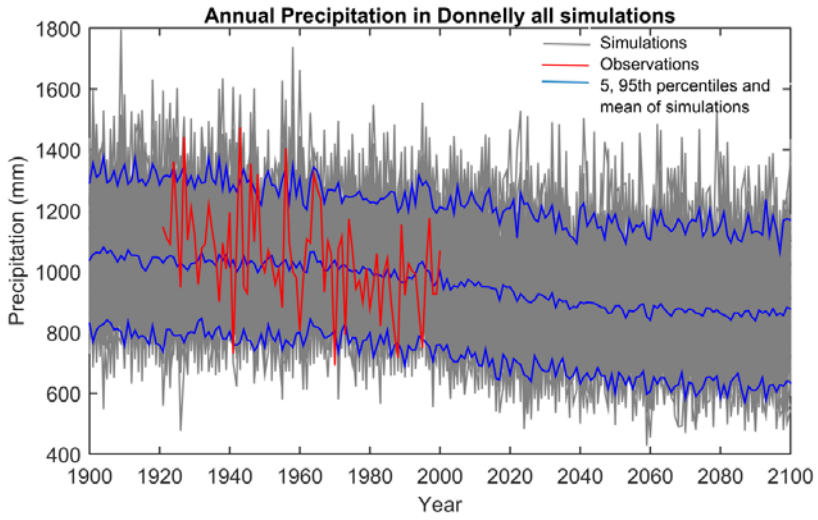

b)

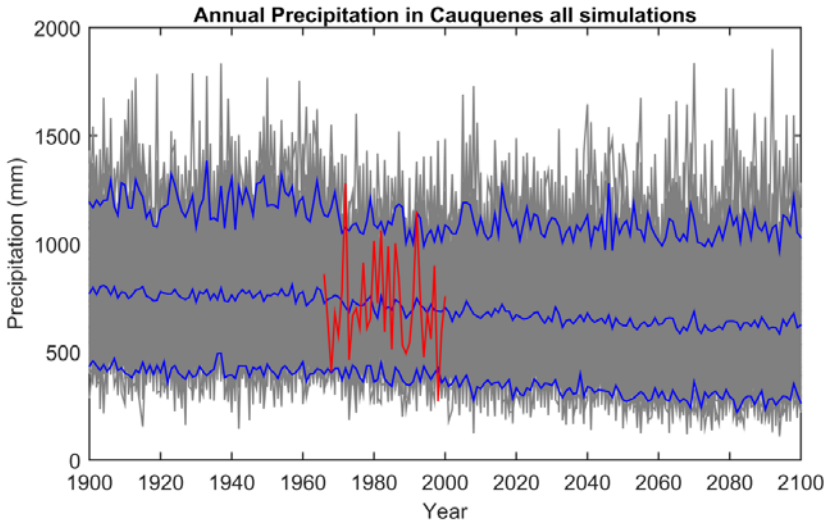

4.2 PERM model calibration and evaluation in SWA and CC catchments

The PERM model was run on a monthly basis and calibrated against annual data for the three SWA catchments using observed area-weighted temperature and rainfall from the AWAP data (Jones et al., 2009). The calibrated parameters and calibration model performance statistics are presented in **Error! Reference source not found.**, while the evaluation of model performance is presented in Table 3. PERM simulates annual runoff well in the three catchments, with a mean coefficient of determination (R^2) of 0.79

and annual Nash & Sutcliffe Efficiency (N&SE) of 0.78. The poorest PERM performance was observed in the driest catchment, Helena River, which is still considered in our analysis because it is one of the most susceptible to climate change as dry catchments are most sensitive to changes in precipitation (Dooge 1992; Dooge et al. 1999; Sankarasubramanian et al. 2001). The N&SE of the K-Fold cross-validation of the model is presented in Table 3, which averaged 0.74 over the three catchments, and indicates that the model is robust at representing the annual hydrology of SWA catchments. The average difference between modelled and observed mean annual runoff and annual coefficient of variation across the three catchments was 2.3 per cent and 3.6 per cent respectively during the calibration period.

PERM was also calibrated for the three CC catchments using monthly observed area-weighted temperature and rainfall data. We found that PERM is accurate at representing the annual hydrology of the CC catchments, with an average coefficient of determination (R^2) of 0.77 and Nash & Sutcliffe Efficiency value (N&SE) of 0.76 across the three catchments during calibration (see Table 2). Regarding the evaluation of PERM, the average N&SE of the K-Fold cross-validation was 0.75 over the three catchments, which indicates the model performs well in these catchments (see Table 3). The average difference between modelled and observed mean annual runoff and annual coefficient of variation across the three catchments was 1.5 per cent and 14 per cent respectively during the calibration period.

Table 2 Calibrated parameters and calibration statistics for PERM in the CC and SWA catchments

Catchment	*Parameters*					*Calibration annual modelled and observed runoff*	
	Smax	*Etrate*	*K*	*Melt*	*Imax*	R^2	*N&SE*
Donnelly River at Strickland	767.81	7.56	0	0.27	23.88	0.94	0.94
Helena River at Ngangaguringuring	200	60	0.41	0.02	100	0.62	0.59
Denmark River at Kompup	936.56	12.22	0.27	0.83	92.75	0.78	0.78
Cauquenes River at el Arrayán	50	3.31	0.85	0.71	121.25	0.82	0.8
Cato River at Puente Cato	154.38	3.69	0.13	0.62	250	0.89	0.87
Lumaco River at Lumaco	1109.69	5.00	0.2	0.83	4.00	0.6	0.6

Table 3 Evaluation of PERM in the CC and SWA catchments

	PERM evaluation results						
Catchment	*Annual N&SE*	*Obs. MAR April-March (mm)*	*Mod. MAR April-March (mm)*	*Dif. Obs and Mod. MAR (%)*	*Obs. Cv April-March*	*Mod. Cv. April-March*	*Dif. Obs. And Mod. CV (%)*
Donnelly River at Strickland	0.7	58.93	57.92	1.70	0.58	0.56	4.83
Helena River at Ngangaguringuring	0.6	6.41	6.1	4.93	0.89	0.88	0.84
Denmark River at Kompup	0.92	162.72	162.98	0.16	0.43	0.41	5.00
Cauquenes River at el Arrayán	0.79	439.93	432.00	1.80	0.60	0.48	20.00
Cato River at Puente Cato	0.86	1301.32	1296.60	0.36	0.38	0.31	18.42
Lumaco River at Lumaco	0.59	624.05	609.43	2.34	0.33	0.31	6.06

4.3 Comparison of the impact of within-GCM and between-GCM uncertainties on runoff projections in SWA catchments

Differences in projected mean annual precipitation and mean annual runoff between the period 2050–2080 and 1970–2000 for the three SWA catchments using first, the ensemble of CPDN GCM runs and then the ensemble of CMIP5 GCM runs were assessed. Histograms of the results for Donnelly catchment using the CPDN (from Barria et al. (2015)) and the two emissions scenarios from CMIP5 are presented in Figure 6. The 2500 runs using CPDN indicate reductions in mean annual precipitation for the period 2050-2080 compared to 1970-2000 with a median of around 21 per cent, which leads to decreases in mean annual runoff of around 50 per cent for the same period. This amplification in the response of runoff to changes in precipitation is known as runoff sensitivity which has been demonstrated to increase when the humidity ratio decreases, such as in the case of dry catchments or during dry months (Dooge, 1992, Dooge et al., 1999, Sankarasubramanian et al., 2001). The projections using the 106 CMIP5 GCM runs under the RCP4.5 scenario indicate a median reduction of around 12.5 per cent in mean annual precipitation for the same period, which leads to a median decrease in mean annual runoff of about 34 per cent. Simulations under the RCP8.5 scenario indicate a median reduction in mean annual precipitation of around 19 per cent, which leads to a median reduction in mean annual runoff of around 46 per cent, which is very similar to the results obtained for the A1B scenario from the CPDN dataset. Similar results to Donnelly are observed for change in mean annual precipitation and mean annual runoff for the period 2050-2080 relative to 1970-2000 for the Helena River and Denmark River using CPDN and CMIP5, which are presented in Table 4. The histograms of mean annual precipitation and runoff changes for these catchments are presented in Figures S6 and S7 respectively.

Figure 6 Histogram of projected difference in mean annual precipitation and runoff for Donnelly at Strickland for the period 2050-2080 compared to 1970-2000 using CPDN and CMIP5 GCMs

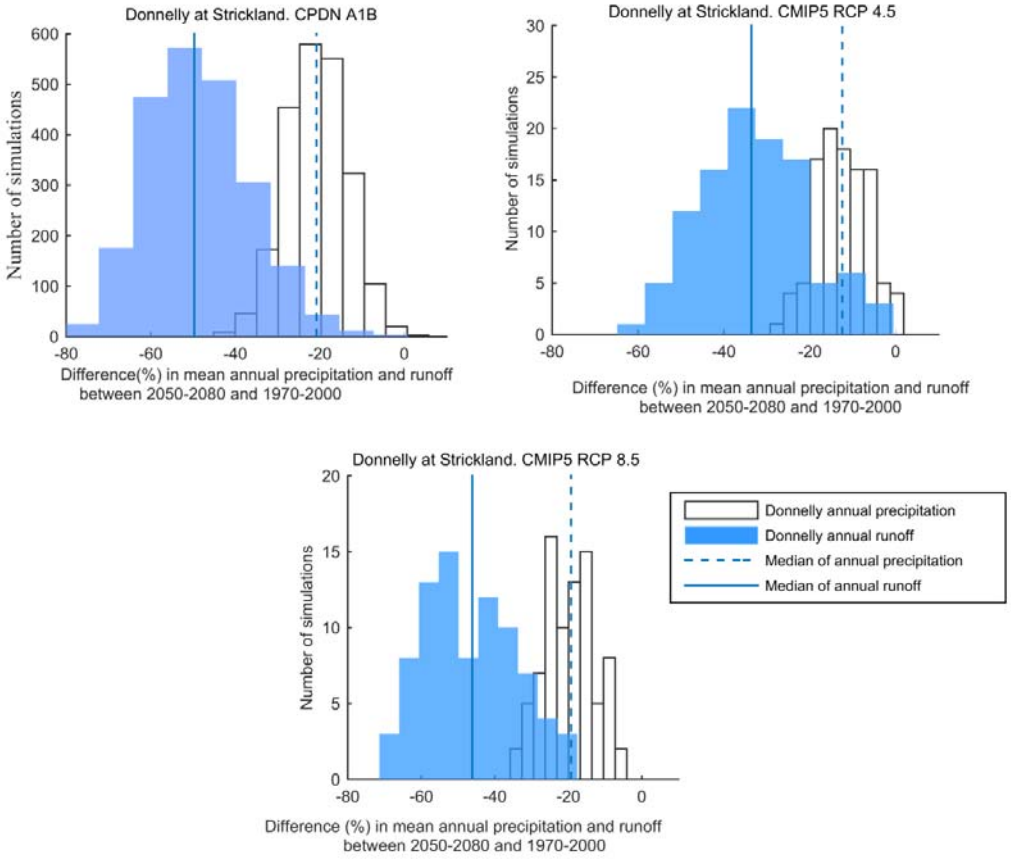

Table 4 Median of the changes in projections of runoff and precipitation for the period between 2050-2080 and 1970-2000 in SWA catchments

Catchment	*Percentile*	*Changes in Precipitation*			*Changes in Runoff*			*Ratio median Runoff/ Prec. CPDN*	*Ratio median Runoff/ Prec. CMIP5 4.5*	*Ratio median Runoff/ Prec. CMIP5 8.5*
		CPDN A1B	*CMIP5 RCP4.5*	*CMIP5 RCP8.5*	*CPDN A1B*	*CMIP5 RCP4.5*	*CMIP5 RCP8.5*			
Donnelly at Strickland	5th	-32.96	-22.47	-31.24	-66.98	-53.48	-64.4	2.39	2.7	2.4
	Median	-20.78	-12.45	-19.26	-49.69	-33.59	-46.13			
	95th	-9.15	-2.19	-8.19	-28.14	-9.05	-26.72			
	Range 5-95th	23.81	20.28	23.05	38.84	44.43	37.68			
Helena at Ngangaguringuring	5th	-36.17	-23.13	-30.22	-84.23	-66.75	-77.66	2.68	2.98	2.86
	Median	-22.59	-12.46	-18.42	-60.45	-37.08	-52.69			
	95th	-8.69	0.75	-2.93	-19.36	16.49	-5.81			
	Range 5-95th	27.48	23.88	27.29	64.87	83.24	71.85			
Denmark at Kompup	5th	-29.45	-18.59	-26.94	-73.99	-56.18	-70.05	2.46	2.75	2.57
	Median	-18.08	-11.08	-16.42	-50.45	-30.49	-42.15			
	95th	-6.72	-0.97	-5.92	-18.15	9	-7.09			
	Range 5-95th	22.73	17.62	21.02	55.84	65.18	62.96			

The quantification of uncertainties in precipitation and runoff projections in the three SWA catchments using the CPDN and the CMIP5 ensembles is presented in Table 4. The results indicate that the within-GCM uncertainty for runoff projections at Donnelly catchment is about 39 per cent (range using CPDN), whereas the mainly between-GCM uncertainty for runoff projections are about 41 per cent (an average of the CMIP5 RCP4.5 and RCP8.5 scenarios). Within-GCM uncertainty for runoff projections at Helena and Denmark catchments of 65 per cent and 56 per cent were obtained, whereas between-GCM uncertainty of 78 per cent and 64 per cent under the CMIP5 RCP4.5 and RCP8.5 scenarios were obtained at Helena and Denmark catchment respectively. The results of the ratio between changes in runoff and changes in precipitation presented in Table 4 indicate that the drier the catchment the more sensitive it is to changes in precipitation. For instance, a given change of 1 per cent in mean annual precipitation in Helena catchment leads to an average reduction of 2.8 per cent in mean annual runoff at Helena catchment.

Results of the Kolmogorov-Smirnov test (not shown) applied to the histograms of changes in projected precipitation and runoff at the three SWA catchments indicate that projections of precipitation and runoff at Donnelly catchment under CPDN and CMIP5 RCP8.5 scenario are from the same distribution at the 5 per cent significance level. Regarding Denmark catchment, the Kolmogorov-Smirnov test indicates that projections of precipitation using CPDN and CMIP5 RCP8.5 scenario are from the same distribution, however the hypothesis is rejected when comparing projections of runoff. Finally, the hypothesis that precipitation and runoff projections under the CPDN and CMIP5 ensemble of GCMs are from the same distribution is rejected at the 5 per cent level of significance at Helena catchment. From these results, we can conclude that the drier the catchment the more independent the simulations of precipitation and runoff obtained using the CPDN and CMIP5 ensembles.

A final comparison is presented in Figure 7, where the mean exceedance probability curve obtained from the ensemble of runoff projections between 2050 and 2080 using CPDN and CMIP5 under the RCP4.5 and RCP8.5 scenarios is shown. The exceedance probability of annual observed runoff is also shown for comparison. The three ensembles of GCMs project reductions in runoff during 2050 and 2080 across all percentiles relative to the observed data. When considering extreme runoff, namely the 5 per cent probability of exceedance runoff and the 95 per cent probability of exceedance runoff, the differences between CPDN and the CMIP5 RCP8.5 scenario ensemble are very small. On average, the difference in the projected 5 per cent probability of exceedance runoff between CPDN and CMIP5 RCP8.5 ensemble is 7 per cent, whereas the difference in the projections of the 95 per cent probability of exceedance runoff is 1 per cent, highlighting the similarities between the projections obtained from these two GCM ensembles.

Figure 7 Exceedance probability of projected mean annual runoff at SWA catchments during 2050-2080

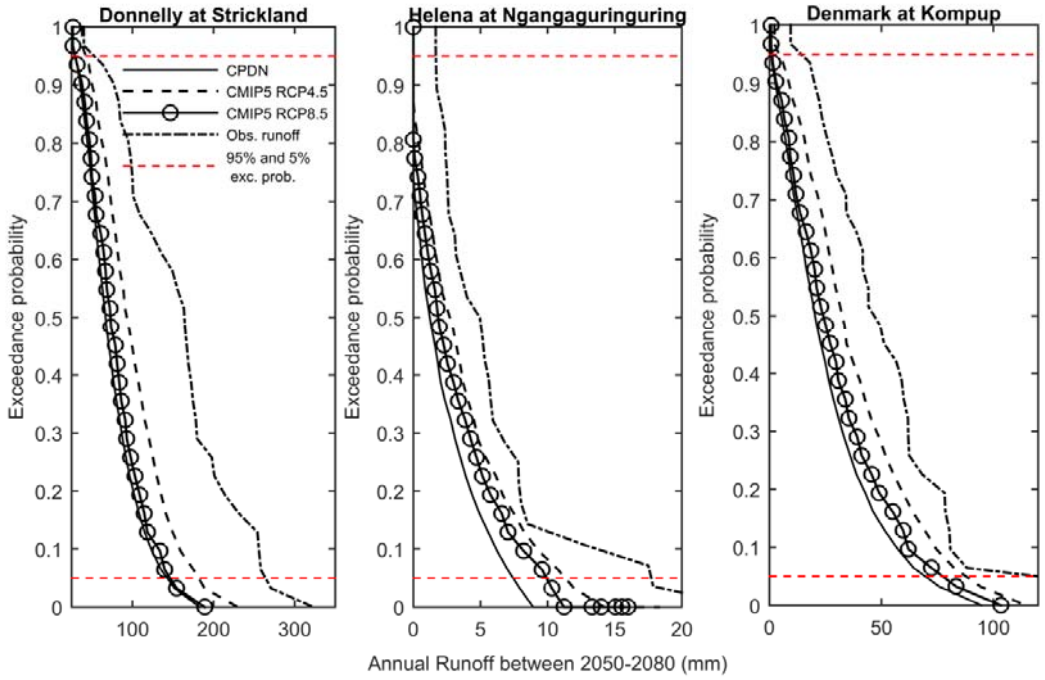

4.4 Between-GCM uncertainty of runoff projections in Central Chilean Catchments

As indicated in the introduction, CPDN is not suitable for projections in CC because the resolution of the output of the model (the Giorgi regions) is too coarse to simulate the complex Chilean topography that helps determine the climate of the region. Therefore, only the effect of between-GCM uncertainty on runoff projections was assessed in this region using the CMIP5 ensemble. Histograms of the percentage change in mean annual precipitation and runoff between 2050-2080 and 1970-2000 obtained from the CMIP5 ensemble under RCP4.5 and RCP8.5 scenarios are presented in Figure 8 for the Cauquenes River. The histograms of Cato and Lumaco River are presented in the supplementary material in Figures S8 and S9 respectively. The 106 runs using CMIP5 RCP4.5 scenario over Cauquenes River indicate a median reduction of around 14 per cent for mean annual precipitation, which leads to a median decrease in mean annual runoff of around 25 per cent. On average, reductions in mean annual precipitation for the period between 2050 and 2080 relative to 1970 and 2000 for the three CC catchments are around 13 per cent which leads to reductions in mean annual runoff of around 21 per cent, with a ratio of change or sensitivity of runoff to changes in precipitation of about 1.6 (Table 5). However, a considerable number of models project increases in precipitation and runoff for the period 2050-2080 compared to 1970-2000, which we further analyse in the following sub-section.

Figure 8 Histogram of projected difference in mean annual precipitation and runoff for Cauquenes at El Arrayan for the period 2050-2080 compared to 1970-2000 using CMIP5 GCMs

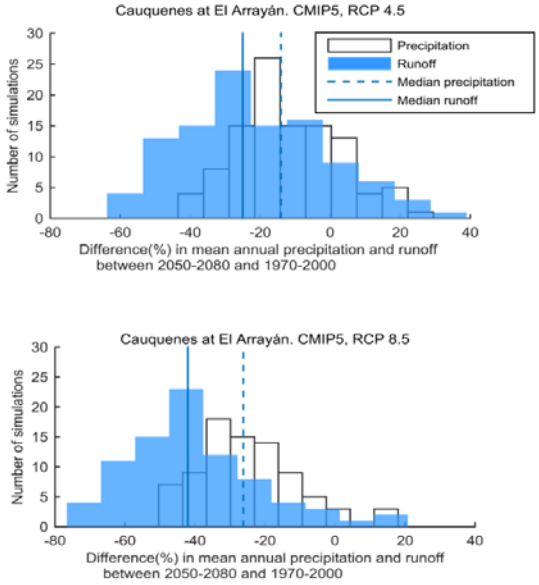

Table 5 Median of the changes in projections of runoff and precipitation for the period between 2050-2080 and 1970-2000 in CC catchments

Catchment	*Percentile*	*Changes in Precipitation*		*Changes in Runoff*		*Ratio median Runoff/Prec. CMIP5 4.5*	*Ratio median Runoff/Prec. CMIP5 8.5*
		CMIP5 RCP4.5	*CMIP5 RCP8.5*	*CMIP5 RCP4.5*	*CMIP5 RCP8.5*		
Cauquenes	5%	-34.92	-45.48	-51.03	-67.4		
	Median	-14.09	-26.19	-25.01	-42.04	1.78	1.61
	95%	15.59	-0.11	17.98	-2.6		
	Dif. 5-95%	50.51	45.37	69.01	64.8		
Lumaco	5%	-31.29	-39.06	-39.56	-51.68		
	Median	-13.05	-21.65	-19.34	-31.8	1.48	1.47
	95%	6.97	-7.46	3.26	-14.61		
	Dif. 5-95%	38.26	31.6	42.82	37.07		
Cato	5%	-30.24	-39.75	-43.51	-59.18		
	Median	-12.22	-22.81	-19.71	-35.72	1.61	1.57
	95%	10.45	0.23	10.91	-7.24		
	Dif. 5-95%	40.69	39.98	54.42	51.94		

The runs using the CMIP5 RCP8.5 scenario over Cauquenes River indicate a median reduction in mean annual precipitation of around 26 per cent, which leads to a median decrease in mean annual runoff of around 42 per cent. The results presented in Table 5 indicate that on average, reductions in mean annual precipitation of about 24 per cent in CC catchments are projected, which leads to reductions in mean annual runoff of about 37 per cent, with a hydrological sensitivity of 1.55, a similar value to that found using the RCP4.5 scenario.

According to the results presented in Table 5, the between-GCM uncertainty in mean annual precipitation in Cauquenes River under the RCP4.5 and the RCP8.5 scenarios are about 51 per cent and 45 per cent respectively. Furthermore, the between-GCM uncertainty in runoff projections at Cauquenes River is about 69 per cent and 65 per cent under the RCP4.5 and RCP8.5 scenarios respectively. Between-GCM uncertainty in CC catchments is very large, with an average across the three catchments of about 55 per cent under the RCP4.5 scenario and of about 51 per cent under the RCP8.5 scenario.

4.5 Analysis of interplay between ozone recovery and GHG in CC catchments

Although runoff projections for CC and for SWA under the RCP4.5 scenario (CMIP5) suggest reductions in the period 2050-2080 compared to 1970-2000 with a median of 22 per cent and 34 per cent respectively, some GCM runs project increases of 20 per cent in mean annual runoff for the same period in CC and SWA. To understand this result, we conducted an exploratory analysis for the catchments to investigate the importance to local climate of the interplay between the rate of ozone recovery and the increase in greenhouse gases (Polvani et al., 2011). All CMIP5 GCMs include the effects of time-varying ozone with stratospheric ozone depletion in the past and stratospheric ozone recovery in the future. Following Eyring et al. (2013), we divided the CMIP5 ensemble members into CHEM and NOCHEM models. The CHEM models have either interactive ozone through a coupled chemical climate model or prescribed stratospheric ozone that varies according to the different RCP scenario used in the GCM (Table S1). In contrast, the NOCHEM models have one prescribed time-varying ozone path that is used for all RCP scenarios. Histograms of percentage change in mean annual runoff for the period 2050-2080 relative to 1970-2000 considering both CHEM and NOCHEM models in the CMIP5 ensemble (RCP4.5 scenario) for CC and SWA catchments are presented in **Error! Reference source not found.** and Figure 10 respectively. According to the Kolmogorov-Smirnov test, there are significant differences between the two groups of models (Chem and NoChem GCMs) for all CC catchments at the 5 per cent level of significance, and only for Denmark catchment in SWA. The CHEM models project a median change in mean annual runoff of -11.6 per cent averaged over the three CC catchments and -30.4 per cent in SWA catchments; while the NOCHEM models project a median change in mean annual runoff of -25.6 per cent and -37 per cent in CC and SWA catchments respectively. Thus, CMIP5 models with interactive or semi-offline ozone (stratospheric ozone levels respond to changes in GHG concentrations) project lesser reductions in mean annual precipitation and hence mean annual runoff for the second half of the century than GCMs with prescribed stratospheric ozone recovery in CC catchments. Fewer differences are observed in SWA catchments, which indicates the sign of reductions is much lesser sensitive to changes in ozone than in CC catchments.

Figure 9 Simulation of runoff under the RCP4.5 scenario using CMIP5 models considering Chem and noChem models in a) Cauquenes River, b) Cato River and c) Lumaco River

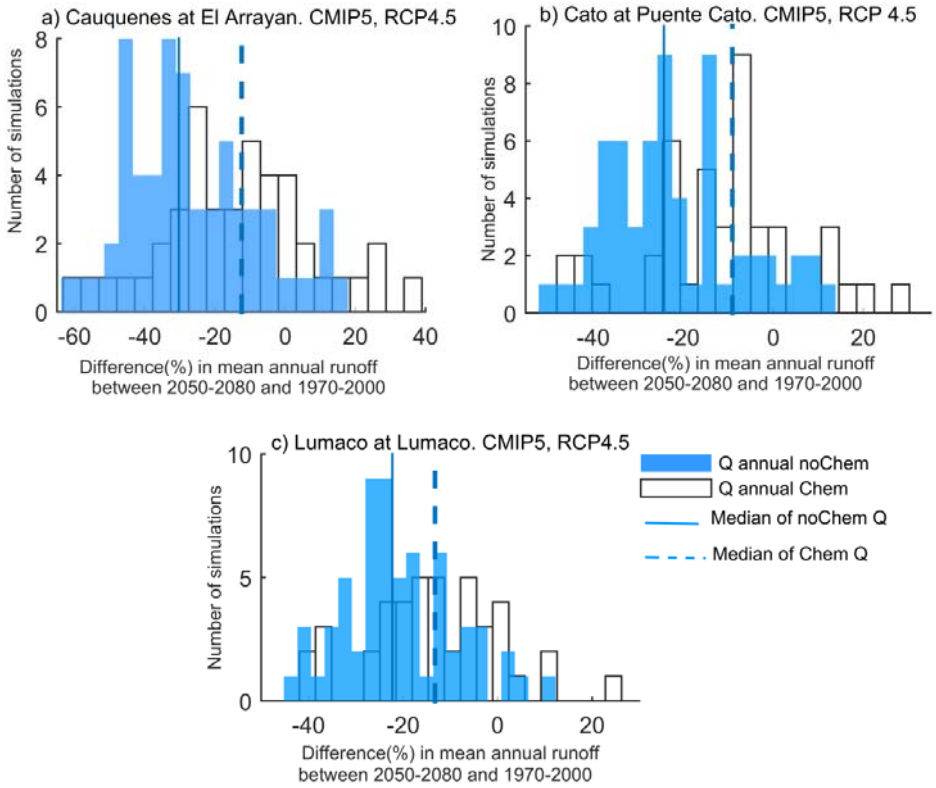

Figure 10 Simulation of runoff under the RCP4.5 scenario using CMIP5 models considering Chem and noChem models in a) Donnelly River, b) Helena River and c) Denmark River

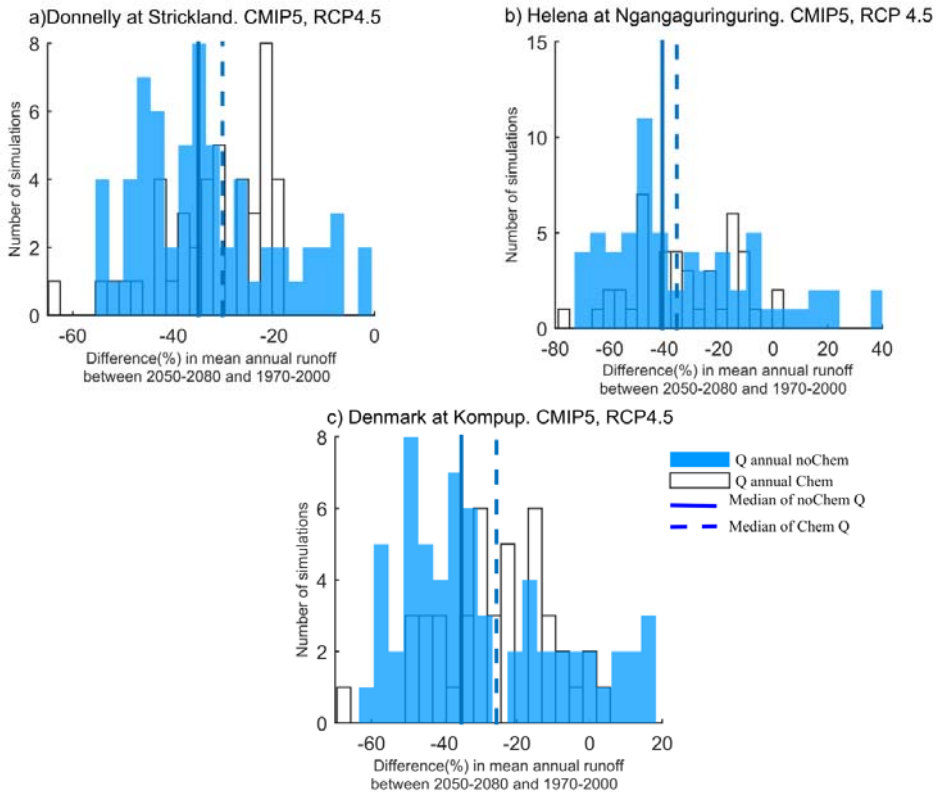

5. Discussion

The results presented in this article indicate that uncertainties in precipitation projections for the second half of the 21st century in SWA and CC catchments are very large (a spread of ~23 per cent and ~40 per cent per cent under the RCP8.5 scenario), which translate into larger uncertainties in runoff projections for the same period (a spread of ~50 per cent in the simulations of both regions).

Regarding the CMIP5 GCM ensemble, most of the runoff simulations under the RCP8.5 scenario suggest reductions during the 21st century with only a few exceptions. In contrast, for the RCP4.5 scenario results are more mixed, with reduced median projections of precipitation and runoff for the period 2050-2080 in the six study catchments, but some CC and SWA projections have an increase in runoff up to 20 per cent relative to the 1970-2000 mean annual runoff.

Analysis of the GCMs used to project CC and SWA runoff under the RCP4.5 scenario suggests the divergence might be related to differences in the structure of the different GCMs, in particular how they prescribe the stratospheric ozone rate recovery. The divergence is observed in the RCP4.5 scenario, which simulates a radiative forcing of 4.5 W/m^2 by the end of the 21st century, whereas it is not observed in the RCP8.5 scenario, which assumes a radiative forcing of 8.5 W/m^2, which might be masking the effect of the ozone recovery in most of models.

According to the results presented in Section 4.5, the CC runoff simulations that use GCMs with prescribed ozone chemistry (independent of the GHG emission scenario) project major reductions in runoff for the second half of the century, whereas models with interactive ozone project lower reductions. We associate

this difference to the well know interplay between the impact of GHG emissions and ozone recovery in the stratosphere on climatic simulations (Polvani et al., 2011, Eyring et al., 2013). The fact that lower runoff reductions are simulated using GCMs with interactive ozone than prescribed ozone chemistry might be related with Eyring et al. (2013) conclusions. The authors indicated that despite CMIP5 models fit climatic observations reasonably, the models with interactive ozone (CHEM) present larger deviations from the observations.

The precipitation reductions in the mid to high latitudes of the Southern Hemisphere, such as SWA and CC, are largely related to the observed positive trend in the SAM, characterised by a poleward displacement of the westerly jet and the consequent poleward movement of the storm track (Lim et al., 2016, Hendon et al., 2007, Meneghini et al., 2007, Gillett et al., 2006, Polvani et al., 2011). Although both Antarctic ozone stratospheric depletion and increases in GHGs have contributed to these changes, the former has been largely reported as the main driver of the climatic changes in the region (Purich and Son, 2012, Gillett et al., 2013, Kang et al., 2011, Lee and Feldstein, 2013). However, stratospheric ozone is projected to recover by the mid-21st century, which is expected to partially offset the impacts of increases in GHGs on SH mid-latitude climate features (Thompson et al., 2011, Barnes et al., 2014, Eyring et al., 2013, Wang et al., 2014).

Furthermore, Neely et al. (2014) found that a coarse temporal resolution of the ozone specified in CMIP5 GCMs, in particular those that don't use an interactive atmospheric chemical coupled model, is related to bias in representing climatic trends in the SH. They highlight the importance of ozone characterisation in climatic projection assessments in the SH. It is important to note that the analysis presented in this article is only exploratory and further work needs to be done to understand the interplay between stratospheric ozone recovery and GHG emissions and their influence over CC and SWA precipitation and runoff. However, it highlights the importance of evaluating scenario adequacy and GCM ensembles when using projections for practical purposes.

6. Conclusions

The analyses presented in this article enhance the findings that warmer and dry conditions are expected to occur in Mediterranean-like catchments of the Southern Hemisphere during the 21st century (Teng et al., 2012, Bozkurt et al., 2017, Demaria et al., 2013, Prosser, 2011, Prudhomme et al., 2014, Samaniego et al., 2009, Vicuña et al., 2013). On average, reductions of about 47 per cent and 37 per cent in mean annual runoff for the period 2050-2080 relative to 1970-2000 are projected under the RCP8.5 scenario for SWA and CC catchments respectively.

According to our results, uncertainties around the precipitation and runoff projections in SWA are very large. Within-GCM uncertainty for runoff projections in three SWA catchments, for the period 2050-2080, range between 39 per cent and 65 per cent. Furthermore, between-GCM uncertainty for runoff projections range between 44 per cent and 83 per cent for the RCP4.5 scenario and about 38 per cent and 72 per cent under the RCP8.5 scenario in SWA catchments for the same period.

Within and between-GCM uncertainties for SWA catchment precipitation simulations are very similar, especially the results obtained from the CPDN (within-GCM uncertainty) and the CMIP5 (mainly between-GCM uncertainty) under the RCP8.5 scenario. Differences between the 95th and the 5th percentile of rainfall simulations are 25 per cent and 24 per cent on average from CPDN and CMIP5 under the RCP8.5 scenario respectively. Regarding runoff projections, on average within and between-GCM uncertainties are 53.2 per cent and 57.5 per cent respectively. We also noted that the drier the catchment the larger the uncertainty in runoff projections and the larger the differences among between-GCM and within-GCM uncertainties. In SWA, Helena catchment is driest and has the largest difference with 65 per cent and 72 per cent of within and between-GCM uncertainties respectively. This might be related to the larger hydrological sensitivity of dry catchments. At Donnelly catchment both the CPDN and CMIP5 RCP8.5 scenario projections are from the same distributions according to the Kolmogorov-Smirnov test, which indicates within and between-GCM uncertainties of runoff projections are of similar magnitude for this catchment. Furthermore, comparison of the projected runoff 5 per cent and 95 per cent probability of exceedance for the period 2050-2080 in SWA from CPDN and CMIP5 GCM ensembles indicates projected extreme runoffs are very similar, with a difference of 1 per cent for the A1B and RCP8.5 scenarios.

Although the CMIP5 ensemble is not a perturbed physics sample of parameterisations, runoff projections and the uncertainty around them are very similar to the within-GCM uncertainty obtained from a perturbed physics ensemble of GCMs in the SWA region. As some GCMs in CMIP5 have multiple runs using different initial conditions, CMIP5 gives some insight into within-GCM uncertainty as well. Given the easy access to CMIP5 runs that represent all regions of the world, we recommend them as a good sample to be used in hydrological assessments.

To our knowledge this article also provides the first quantification and analysis of GCM uncertainty in runoff projections in Central Chile catchments. On average, between-GCM uncertainty in runoff projections of about 55 per cent and 51 per cent was found for the CC catchments under the RCP4.5 and the RCP8.5 scenarios respectively. Central Chilean catchments have a larger spread in runoff projections for the second half of the century than SWA. According to the results, precipitation and runoff is expected to continue decreasing during the whole 21st century in CC.

Additional investigation of runoff projections using CMIP5 in CC and SWA catchments, under the RCP4.5 scenario, revealed differences in sign of projected changes for the second half of the 21st century in CC catchments might be related to differences in the rate of stratospheric ozone recovery in the models. According to our results, the dichotomy in SWA runoff projections can't be attributed to the stratospheric ozone definition. This highlights the importance of an accurate simulation of this feature in GCMs as the interplay between recovery of the ozone layer and increases in GHG influences climatic variability in the Southern Hemisphere.

Finally, it is important to note that uncertainties quantified in this study are limited to uncertainties from GCMs. Uncertainties due to the downscaling methodology used to correct the climatological projections and in the hydrological model used to simulate streamflow are not accounted for in this study. Therefore, the results presented here are likely to underestimate true uncertainty of runoff projections, which should be kept in mind when conducting hydrological climate change impact assessments.

Acknowledgments

The research was funded, in part, by the Australian Research Council (ARC) Centre of Excellence for Climate System Science (grant CE110001028). Additional funds were provided by the scholarship CONICYT Becas Chile. Murray Peel is the recipient of an Australian Research Council Future Fellowship (FT120100130).

References

ALLAN, R.J. and HAYLOCK, M.R. 1993. Circulation features associated with the winter rainfall decrease in southwestern Australia. *Journal of Climate,* 6**,** 1356-1367.

ARDOIN-BARDIN, S., DEZETTER, A., SERVAT, E., PATUREL, J.-E., MAHE, G., NIEL, H. and DIEULIN, C. 2009. Using general circulation model outputs to assess impacts of climate change on runoff for large hydrological catchments in West Africa. *Hydrological Sciences Journal,* 54**,** 77-89.

ASTER 2009. ASTER global DEM validation summary report. *ASTER GDEM Validation Team: METI, NASA and USGS in cooperation with NGA and other collaborators. Accessed January,* 20**,** 2013.

BARNES, E.A., BARNES, N.W. and POLVANI, L.M. 2014. Delayed Southern Hemisphere climate change induced by stratospheric ozone recovery, as projected by the CMIP5 models. *Journal of Climate,* 27**,** 852-867.

BARRIA, P., WALSH, K.J., PEEL, M.C. and KAROLY, D. 2015. Uncertainties in runoff projections in southwestern Australian catchments using a global climate model with perturbed physics. *Journal of Hydrology,* 529**,** 184-199.

BOISIER, J.P., RONDANELLI, R., GARREAUD, R.D. and MUÑOZ, F. 2016. Anthropogenic and natural contributions to the Southeast Pacific precipitation decline and recent megadrought in central Chile. *Geophysical Research Letters,* 43**,** 413-421.

BOSSHARD, T., CARAMBIA, M., GOERGEN, K., KOTLARSKI, S., KRAHE, P., ZAPPA, M. and SCHÄR, C. 2013. Quantifying uncertainty sources in an ensemble of hydrological climate-impact projections. *Water Resources Research,* 49**,** 1523-1536.

BOZKURT, D., ROJAS, M., BOISIER, J.P. and VALDIVIESO, J. 2017. Climate change impacts on hydroclimatic regimes and extremes over Andean basins in central Chile. *Hydrol. Earth Syst. Sci. Discuss.,* 2017**,** 1-29.

CAI, W. and COWAN, T. 2006. SAM and regional rainfall in IPCC AR4 models: Can anthropogenic forcing account for southwest Western Australian winter rainfall reduction? *Geophysical Research Letters,* 33.

CARRASCO, J. F., OSORIO, R. and CASASSA, G. 2008. Secular trend of the equilibrium-line altitude on the western side of the southern Andes, derived from radiosonde and surface observations. *Journal of Glaciology,* 54**,** 538-550.

CHARLES, S., SILBERSTEIN, R., TENG, J., FU, G., HODGSON, G., GABROVSEK, C., CRUTE, J., CHIEW, F., SMITH, I. and KIRONO, D. 2010. Climate analyses for south-west Western Australia. A report to the Australian Government from the CSIRO South-West Western Australia Sustainable Yields Project. CSIRO, Australia.

CHIEW, F., TENG, J., VAZE, J. and& KIRONO, D. 2009. Influence of global climate model selection on runoff impact assessment. *Journal of Hydrology,* 379**,** 172-180.

CHIEW, F.H., VAZE, J., VINEY, N., PERRAUD, J., TENG, J. and POST, D. 2008. Modelling runoff and climate change impact on runoff in 178 catchments in the Murray-Darling Basin using Sacramento and SIMHYD rainfall-runoff models. *Proceedings of Water Down Under 2008,* 87.

CORTÉS, G., VARGAS, X. and MCPHEE, J. 2011. Climatic sensitivity of streamflow timing in the extratropical western Andes Cordillera. *Journal of Hydrology,* 405**,** 93-109.

DELWORTH, T. L. and ZENG, F. 2014. Regional rainfall decline in Australia attributed to anthropogenic greenhouse gases and ozone levels. *Nature Geoscience,* 7**,** 583-587.

DEMARIA, E., MAURER, E., THRASHER, B., VICUÑA, S. and MEZA, F. 2013. Climate change impacts on an alpine watershed in Chile: Do new model projections change the story? *Journal of Hydrology,* 502**,** 128-138.

DOBLER, C., HAGEMANN, S., WILBY, R.L. and STÖTTER, J. 2012. Quantifying different sources of uncertainty in hydrological projections in an Alpine watershed. *Hydrology and Earth System Sciences,* 16**,** 4343-4360.

DOOGE, J., BRUEN, M. and PARMENTIER, B. 1999. A simple model for estimating the sensitivity of runoff to long-term changes in precipitation without a change in vegetation. *Advances in Water Resources,* 23**,** 153-163.

DOOGE, J. C. 1992. Sensitivity of runoff to climate change: A Hortonian approach. *Bulletin of the American Meteorological Society,* 73**,** 2013-2024.

EFRON, B. and TIBSHIRANI, R. J. 1993. An introduction to the bootstrap, volume 57 of Monographs on Statistics and Applied Probability. *Chapmann & Hall*.

EYRING, V., ARBLASTER, J., CIONNI, I., SEDLÁČEK, J., PERLWITZ, J., YOUNG, P., BEKKI, S., BERGMANN, D., CAMERON□SMITH, P. and COLLINS, W. J. 2013. Long□term ozone changes and associated climate impacts in CMIP5 simulations. *Journal of Geophysical Research: Atmospheres,* 118**,** 5029-5060.

FALVEY, M. and GARREAUD, R. 2007. Wintertime precipitation episodes in central Chile: Associated meteorological conditions and orographic influences. *Journal of Hydrometeorology,* 8**,** 171-193.

FALVEY, M. and GARREAUD, R. D. 2009. Regional cooling in a warming world: Recent temperature trends in the southeast Pacific and along the west coast of subtropical South America (1979–2006). *Journal of Geophysical Research: Atmospheres,* 114.

FREDERIKSEN, J.S. and FREDERIKSEN, C. S. 2007. Interdecadal changes in southern hemisphere winter storm track modes. *Tellus A,* 59**,** 599-617.

FUENZALIDA, H., ACEITUNO, P., FALVEY, M., GARREAUD, R., ROJAS, M. and SANCHEZ, R. 2007. Study on climate variability for Chile during the 21st century.

GARREAUD, R. 2009. The Andes climate and weather. *Advances in Geosciences,* 22**,** 3.

GEOSCIENCE AUSTRALIA 2010. SRTM-derived 1 Second Digital Elevation Models Version 1.0. Australian Government.

GILLETT, N., KELL, T. and JONES, P. 2006. Regional climate impacts of the Southern Annular Mode. *Geophysical Research Letters,* 33.

GILLETT, N.P., FYFE, J.C. and PARKER, D.E. 2013. Attribution of observed sea level pressure trends to greenhouse gas, aerosol, and ozone changes. *Geophysical Research Letters,* 40**,** 2302-2306.

GIORGI, F., WHETTON, P.H., JONES, R.G., CHRISTENSEN, J.H., MEARNS, L.O., HEWITSON, B., VONSTORCH, H., FRANCISCO, R. and JACK, C. 2001. Emerging patterns of simulated regional climatic changes for the 21st century due to anthropogenic forcings. *Geophysical research letters,* 28**,** 3317-3320.

GORDON, C., COOPER, C., SENIOR, C.A., BANKS, H., GREGORY, J.M., JOHNS, T.C., MITCHELL, J. F. and WOOD, R. A. 2000. The simulation of SST, sea ice extents and ocean heat transports in a version of the Hadley Centre coupled model without flux adjustments. *Climate dynamics,* 16**,** 147-168.

HAWKINS, E. and SUTTON, R. 2009. The potential to narrow uncertainty in regional climate predictions. *Bulletin of the American Meteorological Society,* 90**,** 1095.

HAWKINS, E. and SUTTON, R. 2011. The potential to narrow uncertainty in projections of regional precipitation change. *Climate Dynamics,* 37**,** 407-418.

HENDON, H.H., THOMPSON, D.W.J. and WHEELER, M.C. 2007. Australian Rainfall and Surface Temperature Variations Associated with the Southern Hemisphere Annular Mode. *Journal of Climate,* 20**,** 2452-2467.

HENNESSY, K., FITZHARRIS, B., BATES, B., HARVEY, N., HOWDEN, S., HUGHES, L., SALINGER, J. and WARRICK, R. 2007. Australia and New Zealand. In 'Climate Change 2007: Impacts, Adaptation and Vulnerability. Contribution of Working Group II to the Fourth Assessment Report of the Intergovernmental Panel on Climate Change'. Eds ML Parry, OF Canziani, JP Palutikof, PJ van der Linden, CE Hanson) pp 507–540. Cambridge University Press: Cambridge, UK.

HOPE, P., ABBS, D., BHEND, J., CHIEW, F., CHURCH, J., EKSTRÖM, M., KIRONO, D., LENTON, A., LUCAS, C. and MCINNES, K. 2015. Southern and South-Western Flatlands Cluster Report. Climate Change in Australia Projections for Australia's Natural Resource Management Regions: Cluster Reports, eds. Ekström, M. et al., CSIRO and Bureau of Meteorology, Australia.

IOCI 2012. Western Australia's weather and climate: a synthesis of Indian Ocean climate initiative stage 3 research. *Australia: CSIRO and BoM*.

JONES, D.A., WANG, W. and FAWCETT, R. 2009. High-quality spatial climate data-sets for Australia. *Australian Meteorological and Oceanographic Journal,* 58**,** 233.

KANG, S.M., POLVANI, L., FYFE, J. and SIGMOND, M. 2011. Impact of polar ozone depletion on subtropical precipitation. *Science,* 332**,** 951-954.

LAFAYSSE, M., HINGRAY, B., MEZGHANI, A., GAILHARD, J. and TERRAY, L. 2014. Internal variability and model uncertainty components in future hydrometeorological projections: The Alpine Durance basin. *Water Resources Research,* 50**,** 3317-3341.

LEE, S. and FELDSTEIN, S.B. 2013. Detecting ozone-and greenhouse gas–driven wind trends with observational data. *Science,* 339**,** 563-567.

LIM, E.P., HENDON, H.H., ARBLASTER, J.M., DELAGE, F., NGUYEN, H., MIN, S.K. and WHEELER, M.C. 2016. The impact of the Southern Annular Mode on future changes in Southern Hemisphere rainfall. *Geophysical Research Letters,* 43**,** 7160-7167.

MAGRIN, G., MARENGO, J., BOULANGER, J., BUCKERIDGE, M., CASTELLANOS, E., POVEDA, G., SCARANO, F. and VICUÑA, S. 2014. Central and South America. *Climate change***,** 1499-1566.

MEEHL, G., COVEY, C., DELWORTH, T., LATIF, M., MCAVANEY, B., MITCHELL, J., STOUFFER, R. and TAYLOR, K. 2007. The WCRP CMIP3 multi-model dataset: A new era in climate change research. *Bulletin of the American Meteorological Society,* 88**,** 1383-1394.

MENEGHINI, B., SIMMONDS, I. and SMITH, I.N. 2007. Association between Australian rainfall and the southern annular mode. *International Journal of Climatology,* 27**,** 109-121.

MILLY, P.C., DUNNE, K.A. and VECCHIA, A.V. 2005. Global pattern of trends in streamflow and water availability in a changing climate. *Nature,* 438**,** 347-50.

MOP 2012. Estrategia Nacional de Recursos Hídricos 2012-2025.

MOSS, R. H., EDMONDS, J.A., HIBBARD, K.A., MANNING, M.R., ROSE, S.K., VAN VUUREN, D.P., CARTER, T.R., EMORI, S., KAINUMA, M., KRAM, T., MEEHL, G.A., MITCHELL, J.F., NAKICENOVIC, N., RIAHI, K., SMITH, S.J., STOUFFER, R.J., THOMSON, A.M., WEYANT, J.P. and WILBANKS, T.J. 2010. The next generation of scenarios for climate change research and assessment. *Nature,* 463**,** 747-56.

MOTE, P., BREKKE, L., DUFFY, P.B. and MAURER, E. 2011. Guidelines for constructing climate scenarios. *Eos,* 92**,** 257-258.

NAKICENOVIC, N., ALCAMO, J., DAVIS, G., DE VRIES, B., FENHANN, J., GAFFIN, S., GREGORY, K., GRUBLER, A., JUNG, T.Y. and KRAM, T. 2000. Special report on emissions scenarios: a special report of Working Group III of the Intergovernmental Panel on Climate Change. Pacific Northwest National Laboratory, Richland, WA (US), Environmental Molecular Sciences Laboratory (US).

NASH, J.E. and SUTCLIFFE, J.V. 1970. River flow forecasting through conceptual models part I—A discussion of principles. *Journal of hydrology,* 10**,** 282-290.

NEELY, R., MARSH, D., SMITH, K.L., DAVIS, S. and POLVANI, L.M. 2014. Biases in southern hemisphere climate trends induced by coarsely specifying the temporal resolution of stratospheric ozone. *Geophysical Research Letters,* 41**,** 8602-8610.

NICHOLLS, N. 2009. Local and remote causes of the southern Australian autumn-winter rainfall decline, 1958–2007. *Climate Dynamics,* 34**,** 835-845.

PARKER, W.S. 2013. Ensemble modeling, uncertainty and robust predictions. *Wiley Interdisciplinary Reviews: Climate Change,* 4**,** 213-223.

PEEL, M., SRIKANTHAN, R., MCMAHON, T. and KAROLY, D. 2015. Approximating uncertainty of annual runoff and reservoir yield using stochastic replicates of global climate model data. *Hydrology and Earth System Sciences,* 19**,** 1615-1639.

PEEL, M.C., FINLAYSON, B.L. and MCMAHON, T.A. 2007. Updated world map of the Köppen-Geiger climate classification. *Hydrology and earth system sciences discussions,* 4**,** 439-473.

POLVANI, L.M., WAUGH, D.W., CORREA, G.J.P. and SON, S.-W. 2011. Stratospheric Ozone Depletion: The Main Driver of Twentieth-Century Atmospheric Circulation Changes in the Southern Hemisphere. *Journal of Climate,* 24**,** 795-812.

PRESTON, B.L. and JONES, R.N. 2008. Evaluating sources of uncertainty in Australian runoff projections. *Advances in Water Resources,* 31**,** 758-775.

PROSSER, I. P. 2011. *Water: science and solutions for Australia*, CSIRO.

PRUDHOMME, C. and DAVIES, H. 2009a. Assessing uncertainties in climate change impact analyses on the river flow regimes in the UK. Part 1: baseline climate. *Climatic Change,* 93**,** 177-195.

PRUDHOMME, C. and DAVIES, H. 2009b. Assessing uncertainties in climate change impact analyses on the river flow regimes in the UK. Part 2: future climate. *Climatic Change,* 93**,** 197-222.

PRUDHOMME, C., GIUNTOLI, I., ROBINSON, E.L., CLARK, D.B., ARNELL, N.W., DANKERS, R., FEKETE, B.M., FRANSSEN, W., GERTEN, D. and GOSLING, S.N. 2014. Hydrological droughts in the 21st century, hotspots and uncertainties from a global multimodel ensemble experiment. *Proceedings of the National Academy of Sciences,* 111**,** 3262-3267.

PURICH, A. and SON, S.-W. 2012. Impact of Antarctic ozone depletion and recovery on Southern Hemisphere precipitation, evaporation, and extreme changes. *Journal of Climate,* 25**,** 3145-3154.

QUINTANA, J. and ACEITUNO, P. 2012. Changes in the rainfall regime along the extratropical west coast of South America (Chile): 30-43º S. *Atmósfera,* 25**,** 1-22.

REISINGER, A., KITCHING, R.L., CHIEW, F., HUGHES, L., NEWTON, P.C.D., SCHUSTER, S.S., TAIT, A. and WHETTON, P. 2014. Australasia. *Climate change,* 1371-1438.

ROWLANDS, D.J., FRAME, D.J., ACKERLEY, D., AINA, T., BOOTH, B.B., CHRISTENSEN, C., COLLINS, M., FAULL, N., FOREST, C.E. and GRANDEY, B.S. 2012. Broad range of 2050

warming from an observationally constrained large climate model ensemble. *Nature Geoscience,* 5**,** 256-260.

RUBIO, E. and MCPHEE, J. 2010. Patterns of spatial and temporal variability in streamflow records in south central Chile in the period 1952–2003. *Water Resources Research,* 46.

SAMANIEGO, J., DE MIGUEL, C.J., GALINDO, L.M., GÓMEZ, J.J., MARTÍNEZ, K. and CETRÁNGOLO, O. 2009. La economía del cambio climático en Chile: síntesis.

SANKARASUBRAMANIAN, A., VOGEL, R.M. and LIMBRUNNER, J.F. 2001. Climate elasticity of streamflow in the United States. *Water Resources Research,* 37**,** 1771-1781.

SILBERSTEIN, R., ARYAL, S., DURRANT, J., PEARCEY, M., BRACCIA, M., CHARLES, S., BONIECKA, L., HODGSON, G., BARI, M. and VINEY, N. 2012. Climate change and runoff in south-western Australia. *Journal of Hydrology,* 475**,** 441-455.

SONNENBORG, T.O., SEIFERT, D. and REFSGAARD, J.C. 2015. Climate model uncertainty vs. conceptual geological uncertainty in hydrological modeling. *Hydrology and Earth System Sciences Discussions,* 12**,** 4353-4385.

STAINFORTH, D.A., AINA, T., CHRISTENSEN, C., COLLINS, M., FAULL, N., FRAME, D.J., KETTLEBOROUGH, J.A., KNIGHT, S., MARTIN, A. and MURPHY, J. 2005. Uncertainty in predictions of the climate response to rising levels of greenhouse gases. *Nature,* 433**,** 403-406.

STEINSCHNEIDER, S., POLEBITSKI, A., BROWN, C. and LETCHER, B.H. 2012. Toward a statistical framework to quantify the uncertainties of hydrologic response under climate change. *Water Resources Research,* 48**,** n/a-n/a.

STOCKER, T., QIN, D., PLATTNER, G.-K., ALEXANDER, L., ALLEN, S., BINDOFF, N., BRÉON, F.-M., CHURCH, J., CUBASCH, U. and EMORI, S. 2013. Technical summary. *Climate Change 2013: The Physical Science Basis. Contribution of Working Group I to the Fifth Assessment Report of the Intergovernmental Panel on Climate Change.* Cambridge University Press.

TAYLOR, K.E., STOUFFER, R.J. and MEEHL, G.A. 2012. An overview of CMIP5 and the experiment design. *Bulletin of the American Meteorological Society,* 93**,** 485.

TENG, J., CHIEW, F.H.S., VAZE, J., MARVANEK, S. and KIRONO, D.G.C. 2012. Estimation of Climate Change Impact on Mean Annual Runoff across Continental Australia Using Budyko and Fu Equations and Hydrological Models. *Journal of Hydrometeorology,* 13**,** 1094-1106.

THEMEßL, M.J., GOBIET, A. and HEINRICH, G. 2012. Empirical-statistical downscaling and error correction of regional climate models and its impact on the climate change signal. *Climatic Change,* 112**,** 449-468.

THOMPSON, D.W., SOLOMON, S., KUSHNER, P.J., ENGLAND, M.H., GRISE, K.M. and KAROLY, D.J. 2011. Signatures of the Antarctic ozone hole in Southern Hemisphere surface climate change. *Nature Geoscience,* 4**,** 741-749.

TIMBAL, B. 2004. Southwest Australia past and future rainfall trends. *Climate Research,* 26**,** 233-249.

TRENBERTH, K.E. and HURRELL, J.W. 1994. Decadal atmosphere-ocean variations in the Pacific. *Climate Dynamics,* 9**,** 303-319.

VAN VUUREN, D.P., EDMONDS, J., KAINUMA, M., RIAHI, K., THOMSON, A., HIBBARD, K., HURTT, G.C., KRAM, T., KREY, V. and LAMARQUE, J.-F. 2011. The representative concentration pathways: an overview. *Climatic change,* 109**,** 5-31.

VIALE, M. and GARREAUD, R. 2015. Orographic effects of the subtropical and extratropical Andes on upwind precipitating clouds. *Journal of Geophysical Research: Atmospheres,* 120**,** 4962-4974.

VICUÑA, S., GIRONÁS, J., MEZA, F.J., CRUZAT, M.L., JELINEK, M., BUSTOS, E., POBLETE, D. and BAMBACH, N. 2013. Exploring possible connections between hydrological extreme events and climate change in central south Chile. *Hydrological Sciences Journal,* 58**,** 1598-1619.

WANG, G., CAI, W. and PURICH, A. 2014. Trends in Southern Hemisphere wind□driven circulation in CMIP5 models over the 21st century: Ozone recovery versus greenhouse forcing. *Journal of Geophysical Research: Oceans,* 119**,** 2974-2986.

WOLDEMESKEL, F., SHARMA, A., SIVAKUMAR, B. and MEHROTRA, R. 2016. Quantification of precipitation and temperature uncertainties simulated by CMIP3 and CMIP5 models. *Journal of Geophysical Research: Atmospheres,* 121**,** 3-17.

XU, H., TAYLOR, R. and XU, Y. 2011. Quantifying uncertainty in the impacts of climate change on river discharge in sub-catchments of the Yangtze and Yellow River Basins, China. *Hydrology and Earth System Sciences,* 15**,** 333-344.

SUPPLEMENTARY MATERIAL

Table S1 List of CMIP5 GCMs characteristics

N°	GCM	Climate modelling centre and location	Ensemble member	Resolution	Reference	Stratospheric Ozone
1	ACCESS1-0	Centre for Australian Weather and Climate Research, Australia	r1i1p1	Atmospheric: 1.875°x1.25°, Ocean: 1°x1°	Dix et al. (2013)	No Chem.
2	ACCESS1-3	Centre for Australian Weather and Climate Research, Australia	r1i1p1	Atmospheric: 1.875°x1.25°, Ocean: 1°x1°	Dix et al. (2013)	No Chem.
3	BNU-ESM	College of Global Change and Earth System Science, Beijing Normal University, China	r1i1p1	Atmospheric: 2.7906°x2.8125°, Ocean: 1°x1°	Ji et al. (2014)	Chem.
4	CCSM4	National Centre for Atmospheric Research, USA	r1i1p1, r2i1p1, r3i1p1, r4i1p1, r5i1p1, r6i1p1	Atmospheric: 0.9424°x1.25°, Ocean: 1°x1°	Meehl et al. (2012)	Chem.
5	CESM1-BGC	Community Earth System Model Contributors	r1i1p1	Atmospheric: 0.9424°x1.25°, Ocean: 1°x1°	Gent et al. (2011)	Chem.
6	CESM1-CAM5	Community Earth System Model Contributors	r1i1p1, r2i1p1, r3i1p1	Atmospheric: 0.9424°x1.25°, Ocean: 1°x1°	Gent et al. (2011)	Chem.
7	CMCC-CMS	Centro Euro-Mediterraneo per I Cambiamenti Climatici, Italy	r1i1p1	Atmospheric:3.7111°x3.75°	Vichi et al. (2011)	No Chem.
8	CMCC-CM	Centro Euro-Mediterraneo per I Cambiamenti Climatici, Italy	r1i1p1	Atmospheric: 0.7484°x0.75°	Vichi et al. (2011)	No Chem.
9	CNRM-CM5	Centre National de Recherches Meteorologiques, France	r1i1p1	Atmospheric: 1.4008°x1.40625°, Ocean: 1°x1°	Voldoire et al. (2013)	Chem.
10	CSIRO-Mk3-6-0	Commonwealth Scientific and Industrial Research Organization in collaboration with Queensland Climate Change Centre of Excellence, Australia	r1i1p1, r2i1p1, r3i1p1, r4i1p1, r5i1p1, r6i1p1, r7i1p1, r8i1p1, r9i1p1, r10i1p1	Atmospheric: 1.8653°x1.875°, Ocean: 1.875°x1.875°	Rotstayn et al. (2012)	No Chem.
11	CanESM2	Canadian Centre for Climate Modelling and Analysis, Canada	r1i1p1, r2i1p1, r3i1p1, r4i1p1, r5i1p1	Atmospheric: 2.7906°x2.8125°, Ocean: 0.9303°x1.1407°	Arora et al. (2011)	No Chem.
12	EC-EARTH	EC-EARTH consortium, Europe	r2i1p1, r8i1p1, r9i1p1, r12i1p1	Atmospheric: 1.1215°x1.125°	Hazeleger et al. (2011)	No Chem.
13	FGOALS-g2	LASG, Institute of Atmospheric Physics, Chinese Academy of Sciences and CESS, Tsinghua University, China	r1i1p1	Atmospheric: 2.7906°x2.8125°, Ocean: 1°x1°	Li et al. (2013)	No Chem.
14	FGOALS-s2	LASG, Institute of Atmospheric Physics, Chinese Academy of Sciences, China, The First Institute of Oceanography, SOA, China	r1i1p1	Atmospheric: 1.6590°x2.8125°, Ocean: 1°x1°	Bao et al. (2013)	No Chem.
15	FIO-ESM	The First Institute of Oceanography, SOA, China	r1i1p1, r2i1p1, r3i1p1	Atmospheric: 2°x2°	Qiao et al. (2013)	No Chem.

16	GFDL-CM3	NOAA Geophysical Fluid Dynamics Laboratory, USA	r1i1p1	Atmospheric: 2°x2.5°, Ocean: 0.3344°x1°	Donner et al. (2011)	Chem.
17	GFDL-ESM2G	NOAA Geophysical Fluid Dynamics Laboratory, USA	r1i1p1	Atmospheric: 2.0225°x2°, Ocean: 0.375°x1°	Dunne et al. (2012)	No Chem.
18	GFDL-ESM2M	NOAA Geophysical Fluid Dynamics Laboratory, USA	r1i1p1	Atmospheric: 2.0225°x2.5°, Ocean: 0.3344°x1°	Dunne et al. (2012)	No Chem.
19	GISS-E2-H-CC	NASA Goddard Institute for Space Studies, USA	r1i1p1	Atmospheric: 2°x2.5°, Ocean: 1°x1°	Schmidt et al. (2006)	No Chem.
20	GISS-E2-H-p1	NASA Goddard Institute for Space Studies, USA	r1i1p1, r2i1p1, r3i1p1, r4i1p1, r5i1p1	Atmospheric: 2°x2.5°, Ocean: 1°x1°	Schmidt et al. (2006)	No Chem.
21	GISS-E2-H-p2 and GISS-E2-H-p3	NASA Goddard Institute for Space Studies, USA	r1i1p2, r1i1p3, r2i1p2, r2i1p3, r3i1p2, r3i1p3, r4i1p2, r4i1p3, r5i1p2, r5i1p3	Atmospheric: 2°x2.5°, Ocean: 1°x1°	Schmidt et al. (2006)	Chem.
22	GISS-E2-R-CC	NASA Goddard Institute for Space Studies, USA	r1i1p1	Atmospheric: 2°x2.5°, Ocean: 1°x1.25°	Schmidt et al. (2006)	No Chem.
23	GISS-E2-R-p1	NASA Goddard Institute for Space Studies, USA	r1i1p1, r2i1p1, r3i1p1, r4i1p1, r5i1p1, r6i1p1	Atmospheric: 2°x2.5°, Ocean: 1°x1.25°	Schmidt et al. (2006)	No Chem.
24	GISS-E2-R-p2 and GISS-E2-R-p3	NASA Goddard Institute for Space Studies, USA	r1i1p2, r1i1p3, r2i1p2, r2i1p3, r3i1p2, r3i1p3, r4i1p2, r4i1p3, r5i1p2, r5i1p3, r6i1p3	Atmospheric: 2°x2.5°, Ocean: 1°x1.25°	Schmidt et al. (2006)	Chem.
25	HadGEM2-AO	National Institute of Meteorological Research, Korea Meteorological Administration, Korea	r1i1p1	Atmospheric: 1.25°x1.875°, Ocean: 1°x1°	Martin et al. (2011)	No Chem.
26	HadGEM2-CC	Met Office Hadley Centre, UK	r1i1p1	Atmospheric: 1.25°x1.875°, Ocean: 1°x1°	Martin et al. (2011)	No Chem.
27	HadGEM2-ES	Met Office Hadley Centre, UK	r1i1p1, r2i1p1, r3i1p1, r4i1p1	Atmospheric: 1.25°x1.875°, Ocean: 1°x1°	Collins et al. (2011)	No Chem.
28	IPSL-CM5A-LR	Institut Pierre Simon Laplace, France	r1i1p1, r2i1p1, r3i1p1, r4i1p1	Atmospheric: 1.8947°x3.75°, Ocean: 2°x2°	Dufresne et al. (2013)	Chem.
29	IPSL-CM5A-MR	Institut Pierre Simon Laplace, France	r1i1p1	Atmospheric: 1.2676°x2.5°, Ocean: 2°x2°	Dufresne et al. (2013)	Chem.
30	IPSL-CM5B-LR	Institut Pierre Simon Laplace, France	r1i1p1	Atmospheric: 1.8947°x3.75°, Ocean: 2°x2°	Dufresne et al. (2013)	Chem.
31	MIROC-ESM-CHEM	Japan Agency for Marine-Earth Science and Technology, Atmosphere and Ocean Research Institute (The University of Tokyo), and National Institute for Environmental Studies, Japan	r1i1p1	Atmospheric: 2.7906°x2.8125°, Ocean: 0.5582°x1.40625°	Watanabe et al. (2011)	Chem.

32	MIROC-ESM	Japan Agency for Marine-Earth Science and Technology, Atmosphere and Ocean Research Institute (The University of Tokyo), and National Institute for Environmental Studies, Japan	r1i1p1	Atmospheric: 2.7906°x2.8125°, Ocean: 0.5582°x1.40625°	Watanabe et al. (2011)	Nochem.
33	MIROC5	Japan Agency for Marine-Earth Science and Technology, Atmosphere and Ocean	r1i1p1, r2i1p1, r3i1p1	Atmospheric:1.4008°x1 .40625°, Ocean: 0.5°x1.40625°	Watanabe et al. (2011)	Nochem.
34	MPI-ESM-LR	Max Planck Institute for Meteorology, Germany	r1i1p1, r2i1p1, r3i1p1	Atmospheric:1.8653°x1 .875°	Giorgetta et al. (2013)	No Chem.
35	MPI-ESM-MR	Max Planck Institute for Meteorology, Germany	r1i1p1, r2i1p1, r3i1p1	Atmospheric:1.8653°x1 .875°	Giorgetta et al. (2013)	No Chem.
36	MRI-CGCM3	Meteorological Research Institute, Japan	r1i1p1	Atmospheric:1.8653°x1 .875°	Yukimoto et al. (2012)	No Chem.
37	NorESM1-ME	Norwegian Climate Centre, Norway	r1i1p1	Atmospheric:1.8947°x2 .5°	Iversen et al. (2013)	Chem.
38	NorESM1-M	Norwegian Climate Centre, Norway	r1i1p1	Atmospheric:1.8947°x2 .5°	Iversen et al. (2013)	Chem.
39	bcc-csm1-1-m	Beijing Climate Center, China Meteorological Administration, China	r1i1p1	Atmospheric:2.7906°x2 .8125°, Ocean: 1°x1°	Wu (2012)	No Chem.
40	bcc-csm1-1	Beijing Climate Center, China Meteorological Administration, China	r1i1p1	Atmospheric:2.7906°x2 .8125°, Ocean: 1°x1°	Wu (2012)	No Chem.
41	inmcm4	Russian Institute for Numerical Mathematics, Russia	r1i1p1	Atmospheric:1.5°x2°, Ocean: 0.5°x1°	Volodin et al. (2010)	No Chem.

Table S2 Chilean meteorological stations used in the calibration of PERM model

Station	Catchment	Latitude (°S)	Longitude (°W)
Mangarral	Cauquenes at El Arrayán	-36.2	-72.3
El Alamo	Cauquenes at El Arrayán	-36.1	-72.4
Tutuven Embalse	Cauquenes at El Arrayán	-35.9	-72.4
Caracol	Cato at Puente Cato	-36.7	-71.4
San Fabián	Cato at Puente Cato	-36.6	-71.5
Diguillín	Cato at Puente Cato	-36.9	-71.6
Coihüeco Embalse	Cato at Puente Cato	-36.6	-71.8

Tranamán	Lumaco at Lumaco	-38.0	-73.0
Parque Nahuelbuta	Lumaco at Lumaco	-37.8	-73.0
Traiguén	Lumaco at Lumaco	-38.3	-72.7
Lumaco	Lumaco at Lumaco	-38.16	-72.90

Figure S3 Seasonal variation of runoff in SWA and CC catchments

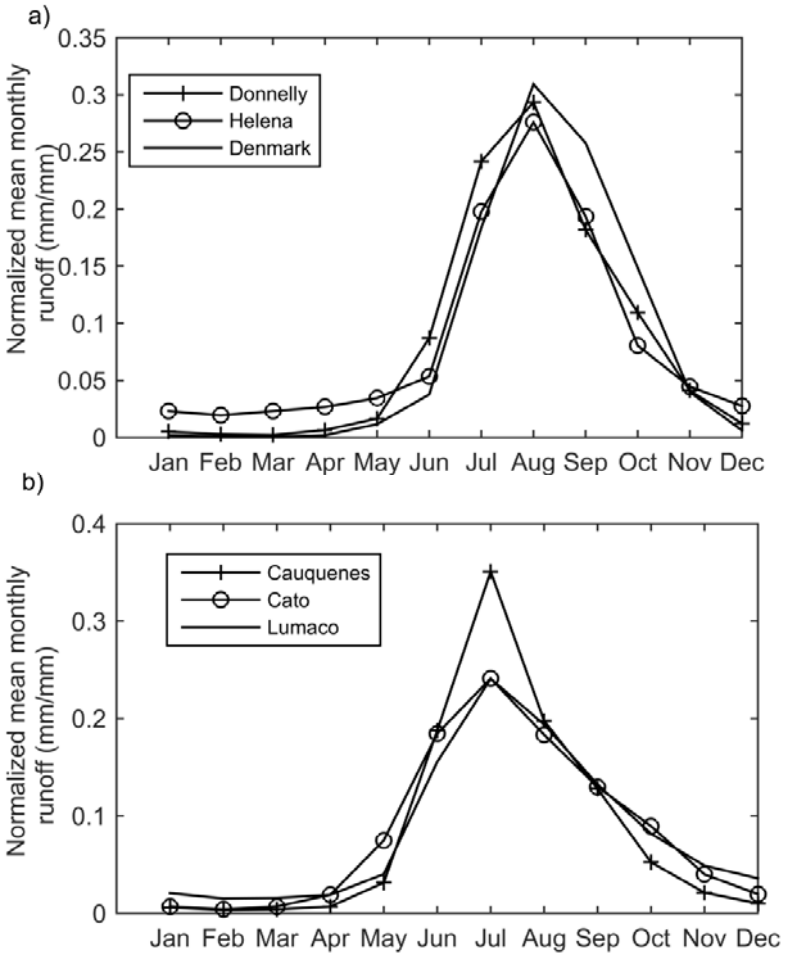

Figure S4 Comparison of mean annual temperature simulated by CMIP5 during the historical period and observed mean annual temperature during the observed period

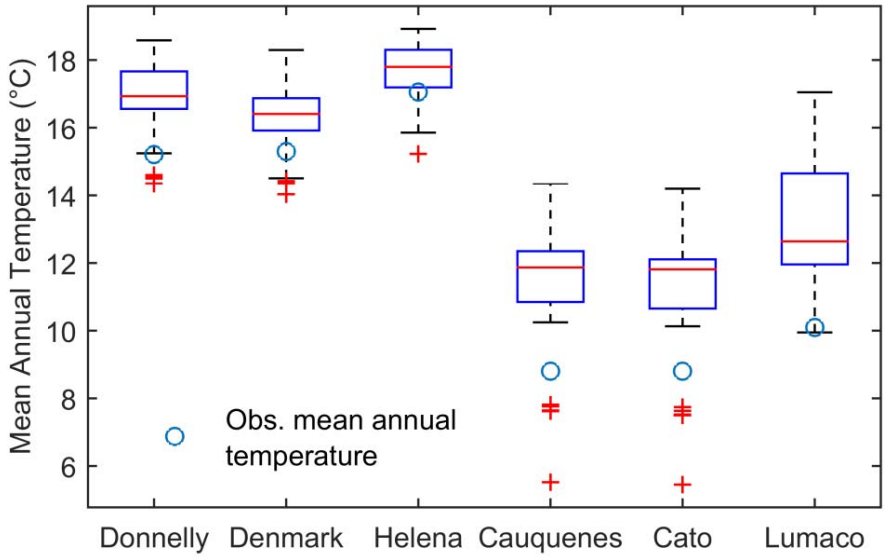

Figure S5 Comparison of standard deviation of annual temperature simulated by CMIP5 during the historical period and the standard deviation of observed annual temperature during the observed period

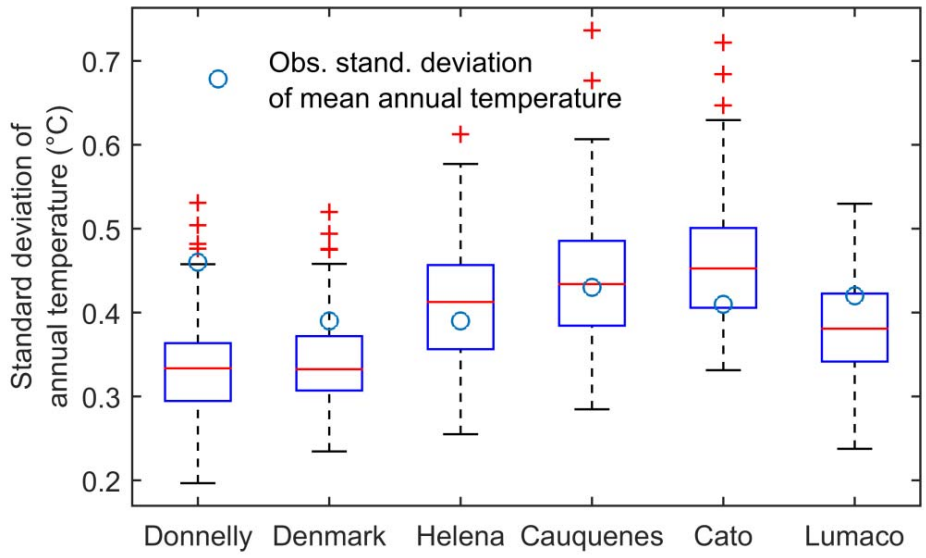

Figure S6 Histogram of projected difference in mean annual precipitation and runoff for Helena at Ngangaguringuring for the period 2050-2080 compared to 1970-2000 using CPDN and CMIP5 GCMs

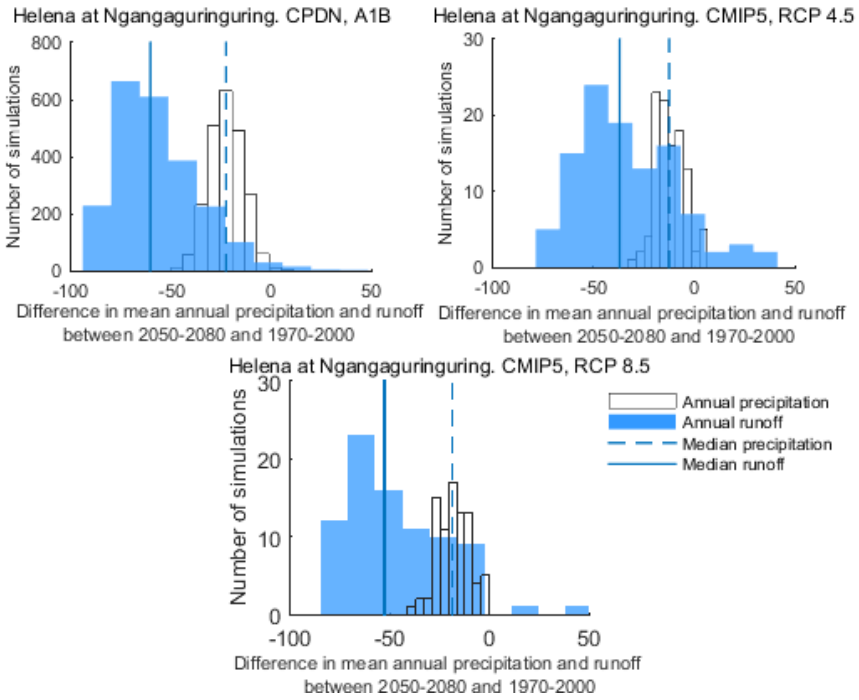

Figure S7 Histogram of projected difference in mean annual precipitation and runoff for Denmark at Kompup for the period 2050-2080 compared to 1970-2000 using CPDN and CMIP5 GCMs

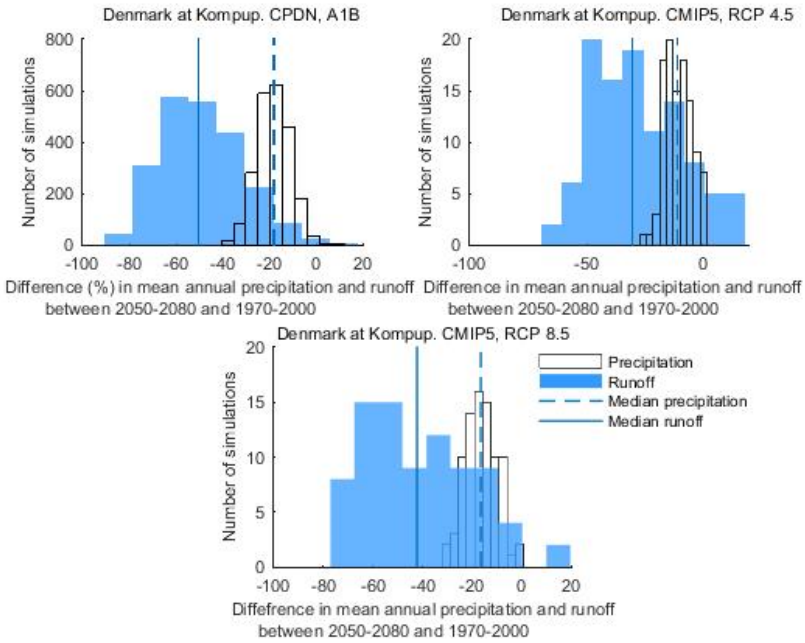

Figure S8 Histogram of projected difference in mean annual precipitation and runoff for Cato in Puente Cato for the period 2050-2080 compared to 1970-2000 using CMIP5 GCMs

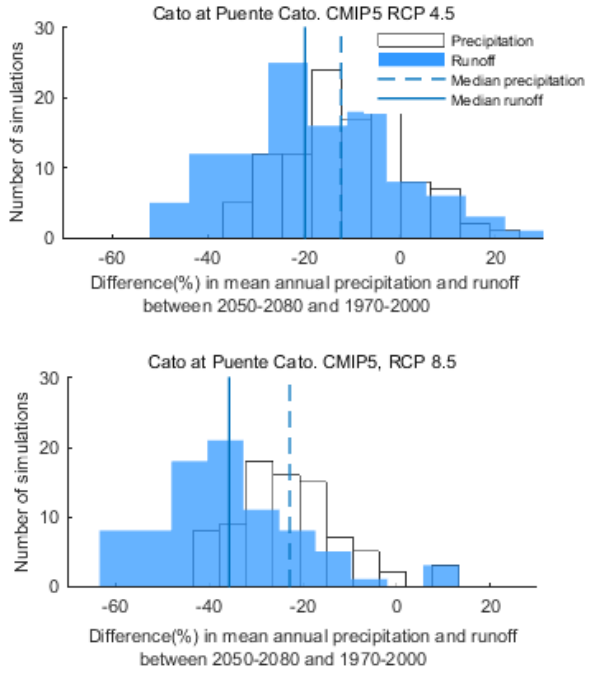

Figure S9 Histogram of projected difference in mean annual precipitation and runoff for Lumaco in Lumaco for the period 2050-2080 compared to 1970-2000 using CMIP5 GCMs